FISEVIER

Contents lists available at ScienceDirect

Earth and Planetary Science Letters

www.elsevier.com/locate/epsl



Inclusions in diamonds constrain thermo-chemical conditions during Mesozoic metasomatism of the Kaapvaal cratonic mantle



Yaakov Weiss a,b,*, Oded Navon b, Steven L. Goldstein a,c, Jeff W. Harris d

- ^a Lamont-Doherty Earth Observatory of Columbia University, Palisades, NY 10964, USA
- ^b The Freddy and Nadine Herrmann Institute of Earth Sciences, The Hebrew University of Jerusalem, Jerusalem 91904, Israel
- ^c Department of Earth and Environmental Sciences, Columbia University, Palisades, NY 10964, USA
- ^d School of Geographical and Earth Sciences, University of Glasgow, Glasgow, G12 8QQ, UK

ARTICLE INFO

Article history: Received 15 August 2017 Received in revised form 5 March 2018 Accepted 9 March 2018 Available online 5 April 2018 Editor: M. Bickle

Keywords:
Kaapvaal craton
sub-continental lithospheric mantle (SCLM)
diamond
high density fluids (HDFs)
thermobarometry
oxygen fugacity (fO₂)

ABSTRACT

Fluid/melt inclusions in diamonds, which were encapsulated during a metasomatic event and over a short period of time, are isolated from their surrounding mantle, offering the opportunity to constrain changes in the sub-continental lithospheric mantle (SCLM) that occurred during individual thermochemical events, as well as the composition of the fluids involved and their sources. We have analyzed a suite of 8 microinclusion-bearing diamonds from the Group I De Beers Pool kimberlites, South Africa, using FTIR, EPMA and LA-ICP-MS. Seven of the diamonds trapped incompatible-element-enriched saline high density fluids (HDFs), carry peridotitic mineral microinclusions, and substitutional nitrogen almost exclusively in A-centers. This low-aggregation state of nitrogen indicates a short mantle residence times and/or low mantle ambient temperature for these diamonds. A short residence time is favored because, elevated thermal conditions prevailed in the South African lithosphere during and following the Karoo flood basalt volcanism at \sim 180 Ma, thus the saline metasomatism must have occurred close to the time of kimberlite eruptions at \sim 85 Ma. Another diamond encapsulated incompatible-element-enriched silicic HDFs and has 25% of its nitrogen content residing in B-centers, implying formation during an earlier and different metasomatic event that likely relates to the Karoo magmatism at ca. 180 Ma.

Thermometry of mineral microinclusions in the diamonds carrying saline HDFs, based on Mg–Fe exchange between garnet–orthopyroxene (Opx)/clinopyroxene (Cpx)/olivine and the Opx–Cpx thermometer, yield temperatures between 875–1080 °C at 5 GPa. These temperatures overlap with conditions recorded by touching inclusion pairs in diamonds from the De Beers Pool kimberlites, which represent the mantle ambient conditions just before eruption, and are altogether lower by 150–250 °C compared to P-T gradients recorded by peridotite xenoliths from the same locality. Oxygen fugacity (fO₂) differs as well. The fO₂ calculated for the saline HDF compositions (Δ log fO_{2(FMQ)} = -2.47 to -1.34) are higher by about a log unit compared with that recorded by xenoliths at 4–7 GPa.

We conclude that enriched saline HDFs mediated the metasomatism that preceded Group I kimberlite eruptions in the southwestern Kaapvaal craton, and that their 'cold and oxidized' nature reflects their derivation from a deep subducting slab. This event had little impact on the temperature and redox state of the Kaapvaal lithosphere as a reservoir, however, it likely affected its properties along limited metasomatized veins and their wall rock. To reconcile the temperature and oxygen fugacity discrepancy between inclusions in diamonds and xenoliths, we argue that xenoliths did not equilibrate during the last saline metasomatic event or kimberlite eruption. Thus the $P-T-fO_2$ gradients they record express pre-existing lithospheric conditions that were likely established during the last major thermal event in the Kaapvaal craton (i.e. the Karoo magmatism at ca. 180 Ma).

© 2018 Elsevier B.V. All rights reserved.

1. Introduction

Constraining thermo-chemical changes in the sub continental lithospheric mantle (SCLM), which influence its density and stability (e.g. Baptiste and Tommasi, 2014; Carlson et al., 2005; Deen et al., 2006), rheology (e.g. Eaton et al., 2009) and oxidation

E-mail address: yweiss@ldeo.columbia.edu (Y. Weiss).

^{*} Corresponding author at: Lamont-Doherty Earth Observatory of Columbia University, Palisades, NY 10964, USA.

state (e.g. Luth and Stachel, 2014; Tappe et al., 2007), is a major on-going challenge in mantle geodynamics. Direct samples of the mantle (xenoliths and xenocrysts) provide information on the timing of such temporal modifications, the depth within the lithosphere where changes took place, and the temperature and chemical/mineralogical modifications that occurred during such events (e.g. Lazarov et al., 2009a, 2012; Simon et al., 2007). In most cases fluid-rock interaction during metasomatism is the driving force for alteration, but remnants of the metasomatic agent involved are only rarely observed (e.g. van Achterbergh et al., 2002). The nature of mantle metasomatic fluids must therefore be inferred indirectly, from geochemical proxies or calculated using mineral/melt partition coefficients. Also, as a consequence of complexities from chemical overprinting of sub cratonic mantle rocks by multiple alteration/enrichment events over time, there is ongoing debate whether metasomatism was accomplished by interaction with low density C-O-H fluids or melts having various possible compositions and redox states. Other important related issues include the effects of such interactions on the rock lithologies and chemical compositions, and the linkages existing between the mantle sources of the fluids/melts involved in metasomatism and regional tectonic episodes.

The SCLM of the southwestern part of the Kaapvaal Craton in South Africa has been studied intensively. Mantle derived xenoliths and xenocrysts from this area document intensive chemical depletion by melting during the Archean, with up to >40% melt extraction (e.g. Griffin et al., 2003; Kelemen et al., 1998; Pearson et al., 1995), followed by a complex metasomatic history that is related to several tectonic and magmatic events. Archean enrichment in SiO₂, light rare earth elements (LREEs) and large ion lithophile elements (LILE: K, Ba, Ca, Sr) is attributed to hydrous fluids and silicate and carbonatitic melts released from subducting slabs during and after amalgamation of the Kimberley and Witwatersrand blocks, at ca. 2.9 Ga (e.g. Bell et al., 2005; Shirey et al., 2004; Simon et al., 2007), and continuing until the final stabilization of the craton at ~ 2.6 Ga (Lazarov et al., 2009a, 2012). During the Proterozoic and early Phanerozoic, three phases of metasomatism, thought to be induced by subduction-derived aqueous fluids and/or silicic-carbonatitic melts that formed in-situ within a previously metasomatized SCLM, are recorded at 1.9 ± 0.2 Ga, 1.3 ± 0.4 Ga and 0.4 ± 0.12 Ga (e.g. Lazarov et al., 2009a, 2012). The timings of alteration coincide with the Kheis-Magondi orogeny at 1.93-1.89 Ga (Armstrong, 1987), the Namaqua-Natal orogeny at 1.2-1 Ga (Pettersson et al., 2007) and the formation of the Damara belts and their attachment to the craton at \sim 500 Ma (Gray et al., 2008). 'Young' metasomatism, which involved enrichment of the SCLM in high-field-strength elements (HFSE; Ti, Zr, Hf, Nb), LILE and LREE and the formation of pyroxene, phlogopite, amphibole, Fe-Ti oxides and LIMA (lindsleyite-mathiasite) phases, has been attributed to Mesozoic magmatism (e.g. Giuliani et al., 2014; Simon et al., 2007) of both the Karoo flood basalt (175-185 Ma, Jourdan et al., 2007) and the eruptions of Group II and Group I kimberlites (mainly at \sim 125 \pm 10 and 85 \pm 5 Ma, respectively) (Field et al., 2008 and references therein).

Along with the chemical modifications, mantle metasomatism is responsible for thermal perturbations and changes in the oxygen fugacity (fO_2) of the SCLM. Mantle xenoliths and xenocrysts are likely to record changes mainly due to the last metasomatic event, before their sampling and ascent in kimberlitic magmas. For example, xenoliths from the Kaapvaal lithosphere mostly cluster along a temperature-depth calculated geotherm for continental shield regions (40–42 mW/m², e.g. Rudnick, 1999); while thermally perturbed xenoliths from depths greater than 150 km (>5 GPa) are displaced to higher temperatures, away from the general P–T gradient, and are characterized by textural deformation and incom-

patible element enrichment (Bell et al., 2003; Boyd and Gurney, 1986). These thermal variations in the Kaapvaal SCLM are interpreted as the result of Cretaceous metasomatism that occurred during the time frame between the eruption episodes of the Group II and Group I kimberlites (Bell et al., 2003; Griffin et al., 2003; Kobussen et al., 2009). Associated garnet peridotite xenoliths provide evidence for an fO2 increase during metasomatism, by up to ~ 2 $\Delta \log$ units in the most incompatible element enriched samples from the southwestern province of the Kaapvaal (e.g. Creighton et al., 2009; Woodland and Koch, 2003). Among these, the recorded increase in fO2 along compositional changes from core to rim in some xenolithic zoned garnets is estimated to take place within <1 Ma of kimberlite eruption (Griffin et al., 1999: McCammon et al., 2001; Berry et al., 2013). The change in fO_2 approaches the enstatite + magnesite = forsterite + graphite/diamond $+ O_2$ (EMOG/D) reaction curve (Eggler and Baker, 1982), suggesting the involvement of oxidized fluid/melt during metasomatism

Here we focus on the recent metasomatic events that took place at the southwestern Kaapvaal SCLM, prior to, and between, the Mesozoic kimberlite eruption episodes. However rather than investigating the chemical changes of lithospheric rocks and inferring the metasomatic agents involved, we look directly at the melts or super critical-end-point fluids (HDFs, high density fluids) responsible for alteration, by analyzing the composition of micrometer-size inclusions in diamonds. We report the major- and trace-element data for a suite of eight such microinclusion-bearing diamonds from the De Beers Pool kimberlites (a cluster of four kimberlites in Kimberley, South Africa). These diamonds encapsulate both HDF and mineral microinclusions, allowing us to constrain the composition of the metasomatic agent, the nature of the diamond host rock and the thermal and fO2 conditions during fluid-rock interaction. Combining our data and results on mineral inclusions in monocrystalline diamonds and garnet-bearing peridotite xenoliths from De Beers Pool and related kimberlites in the southwestern Kaapvaal, we discuss the source and evolution of the metasomatic agent, constrain the timing of alteration and diamond growth and, evaluate the impact of Mesozoic metasomatism and volcanism on the thermal and redox state of the provenance lithosphere.

2. Samples and analytical techniques

A suite of eight diamonds from the De Beers Pool kimberlites, South Africa, was selected for the present study. The diamonds have large range in size with weight varying between 14-120 mg. Seven diamonds show cube-like morphology and one (ON-DBP-338) is a coated diamond. The samples vary in color (whitegray-black-green) and carry abundant microinclusions. Three of the diamonds (ON-DBP-330, 335, 337) show a clear distinction between an inner and outer part, characterized with different hue and cathodoluminescence (CL) intensities (Fig. 1 and Supplementary Fig. S1). Each diamond was laser-cut twice to create a thin slab that was polished on both sides. It was then cleaned ultrasonically in a mixture of HF 60% and HNO3 69% for 2 h and washed with ethanol and distilled water before analysis. Electron probe microanalyses (EPMA), Fourier-transform infrared (FTIR) and laser ablation ICP-MS analyses were performed for collecting data on the nitrogen concentration and aggregation states in the different diamonds, and the major and trace element composition and volatile content of the microinclusions they carry. Full analytical techniques are presented in Supplementary Material - Analytical Methods.

Table 1Nitrogen content in ppm and aggregation state of the De Beers Pool diamonds.

Sample	ON-DBP-330		ON-DBP-332	ON-DBP-335	ON-DBP-336	ON-DBP-337	ON-DBP-338
	Inner	Outer					
Total N (ppm)	394	645	640	660	≈0	73	190
%N as B ^a	0	0	25	≈0 (1.6) ^b	_	0	≈0 (4.1)
Mantle residence	time in Myr ^c						
900 °C	>4500	>4500	>4500	>4500	_	>4500	>4500
1000°C	1330	812	>4500	793	-	>4500	2750
1150°C	1.6	1.0	329 ^d	1.0	_	8.7	3.3

- ^a Percentage of nitrogen that is present as B-centers, i.e. five C atoms replaced by four N atoms and a vacancy.
- b In two cases, where no B-centers characteristics were observed in the IR spectrum, the percent of B-centers given by DiaMap was higher than 0.
- ^c Calculated using the calibration of Leahy and Taylor (1997); %N as B=0.1 was used for pure type IaA diamonds (%N as $B\approx0$).
- $^{\rm d}$ At 1180 °C, the mantle residence time of ON-DBP-332 is 101 Myr.

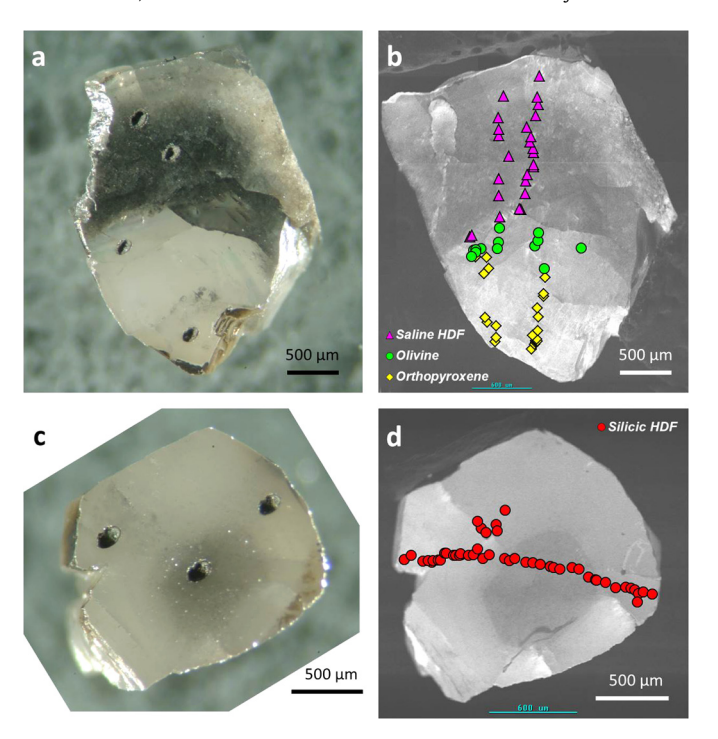


Fig. 1. Two microinclusion-bearing diamonds from the De Beers Pool kimberlites. (a) Diamond ON-DBP-330 showing distinction between a white translucent inner part and an opaque black-gray-white outer part with a sugary texture; the transition between the two parts is sharp. (b) Cathodoluminescence (CL) image of ON-DBP-330 showing the location and type of microinclusions that were analyzed by EPMA. Olivine and orthopyroxene microinclusions were found only at the inner part of this diamond, while the outer part exclusively contains high-density fluid (HDF) microinclusions of saline composition. (c) Diamond ON-DBP-332. (d) CL image of ON-DBP-332 showing the location of HDF microinclusions of silicic composition. Pits in (a) and (c) were excavated during laser ablation ICP-MS analysis. Additional photomicrograph and CL images of De Beers Pool diamonds, that were analyzed in the present study, are presented in Supplementary Fig. S1.

3. Results

3.1. Nitrogen impurities and included material – FTIR spectroscopy

The De Beers Pool diamonds carry 0 to 660 ppm nitrogen in their lattice (Table 1), similar to concentrations detected in other South African fluid-rich diamonds (e.g. Izraeli et al., 2001). Diamond ON-DBP-336 is a Type IIa diamond; this is the first report of a fluid-rich diamond carrying no nitrogen impurities (Supplementary Fig. S2). Four diamonds (ON-DBP-330, 335, 337, 338) exhibit pure Type IaA spectrum and carry nitrogen in A-centers solely, while diamond ON-DBP-332 reveals a Type IaAB with 25% of its nitrogen in B-centers. It also has an associated platelet band at 1373 cm⁻¹ (Fig. 2 and Supplementary Fig. S2, Table 1). This differ-

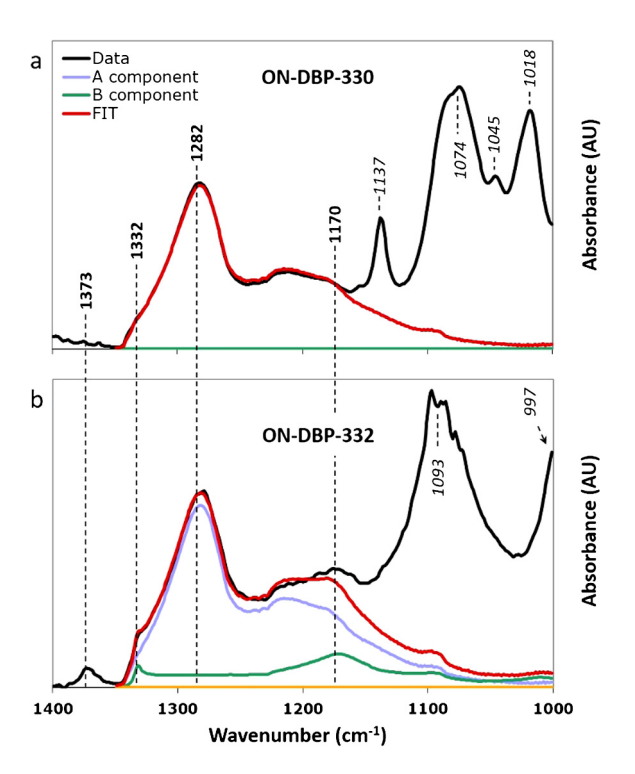


Fig. 2. Infrared absorbance spectra between 1000–1400 cm⁻¹ of the diamonds shown in Fig. 1: (a) the inner part of diamond ON-DBP-330 and (b) diamond ON-DBP-332. Diamond ON-DBP-330 shows nitrogen absorption in A-centers only (main absorbance at 1282 cm⁻¹); ON-DBP-332 has both A- and B-centers, with 25% of the nitrogen in B-centers (main peaks at 1332 and 1170 cm⁻¹). The spectrum also shows absorbance due to nitrogen platelets at 1373 cm⁻¹. Orthopyroxene related absorbance peaks at 1137, 1074, 1045 and 1018 cm⁻¹ are observed in the inner part of ON-DBP-330. In ON-DBP-332, the absorbance peaks at 1093 and 997 cm⁻¹ are related to secondary quartz and mica that grew during cooling of the silicic HDF. See Supplementary Fig. S2 for the full spectra of De Beers Pool diamonds analyzed, and text for additional information.

ence indicates a longer mantle residence time or higher ambient temperature for ON-DBP-332 (Taylor et al., 1990). Diamonds ON-DBP-331 and ON-DBP-339 are opaque and no IR spectrum could be collected.

Previous studies have shown that both primary mineral microinclusions and HDF microinclusions (including various daughter mineral phases and a residual low-density hydrous solution) contribute to the IR absorbance in fluid-rich diamonds (e.g. Navon et al., 1988; Tomlinson et al., 2006). In diamonds ON-DBP-337, ON-DBP-338 and the outer parts of ON-DBP-330 and ON-DBP-335, HDF microinclusions show the absorbance of water (IR bands center at \sim 3440 and 1650 cm $^{-1}$), carbonate (i.e. magnesite, \sim 1450, 880 and 750 cm $^{-1}$) and apatite (\sim 1095, 1060 and 605 cm $^{-1}$) (Fig. 2 and Supplementary Fig. S2). The microinclusions are water-rich with calculated carbonate/(carbonate + water) molar ratio (CMF)

Table 2Average composition of HDF microinclusions in the De Beers Pool diamonds.

Diamond Morphology	ON-DBP-330 Cube-like	ON-DBP-331 Cube-like	ON-DBP-332 Cube-like	ON-DBP-335 Cube-like	ON-DBP-336 Cube-like	ON-DBP-337 Cube-like	ON-DBP-338 Coated	ON-DBP-339 Cube-like
Fluid type	Saline	Saline	Silicic	Saline	Saline	Saline	Saline	Saline
No. of inclusions analyzed	26	50	50	38	9	68	49	57
Composition normalized to 100 wt.% on a water and carbonate free basis, with excess oxygen for chlorine								
SiO ₂ ^a	1.9 (1.0)	1.5 (0.9)	47.9 (4.4)	1.3 (0.9)	4.4 (1.2)	1.5 (1.2)	1.5 (1.1)	3.4 (1.5)
TiO ₂	0.3 (0.5)	0.3 (0.7)	1.1 (0.9)	0.2 (0.4)	1.1 (1.3)	0.3 (0.5)	0.5 (0.8)	0.5 (0.9)
Al_2O_3	0.7 (0.6)	0.9 (0.7)	6.1 (1.1)	0.8 (0.6)	1.4 (1.1)	0.8 (1.0)	0.7 (0.7)	1.6 (1.1)
FeO	4.7 (3.0)	4.8 (2.5)	7.1 (1.7)	5.2 (3.7)	5.4 (1.5)	5.5 (3.0)	8.7 (3.2)	5.1 (2.5)
MgO	3.0 (2.6)	2.5 (1.9)	5.8 (1.1)	2.6 (1.8)	5.1 (1.6)	1.1 (1.0)	1.4 (1.4)	3.2 (2.3)
CaO	10.4 (3.3)	8.9 (3.3)	3.7 (3.0)	10.3 (3.0)	6.3 (1.7)	7.4 (3.6)	8.8 (3.7)	7.2 (4.2)
BaO	1.2 (1.9)	0.6 (0.9)	1.8 (1.8)	0.5 (0.8)	1.2 (1.5)	1.2 (1.4)	4.4 (3.3)	1.2 (3.2)
Na ₂ O	22.4 (5.4)	23.8 (7.6)	1.0 (1.1)	19.9 (5.7)	25.0 (3.1)	24.3 (6.8)	13.0 (6.4)	27.6 (5.1)
K ₂ O	27.2 (5.8)	27.2 (8.8)	18.5 (1.8)	31.5 (7.8)	22.0 (3.4)	27.0 (7.0)	31.2 (6.5)	23.9 (5.6)
P_2O_5	1.0 (0.8)	0.7 (0.6)	5.0 (1.9)	0.8 (0.9)	1.9 (1.3)	0.6 (0.8)	0.5 (0.9)	0.6 (0.7)
Cl	34.8 (7.7)	37.1 (6.2)	2.6 (0.8)	34.4 (4.6)	33.9 (3.4)	38.9 (3.9)	37.7 (2.9)	33.0 (6.1)
Total ^b	8.8 (3.6)	8.7 (3.8)	6.0 (2.7)	9.6 (5.3)	2.0 (0.5)	8.2 (4.2)	8.0 (5.6)	6.0 (2.7)
CMF ^c	0.12 {0.15}	0.15 {0.18}	_	0.12 {0.15}	0.15 {0.18}	0.22 {0.25}	0.12 {0.15}	0.15 {0.18}
CO ₂ ^d	11.0 {11.9}	11.2 {11.8}	-	11.2 {12.1}	10.5 {11.0}	11.1 {11.4}	9.1 {9.7}	12.0 {12.8}
H_2O^e	33.0 {27.5}	27.0 {22.8}	-	33.6 {28.1}	25.3 {21.3}	16.1 {14.0}	27.3 {22.5}	29.0 {24.6}
$X_{CO_2}^{f}$	0.07 {0.08}	0.07 {0.08}	-	0.07 {0.08}	0.07 {0.08}	0.08 {0.08}	0.06 {0.07}	0.08 {0.09}
μ -mineral assemblage	Ol + Opx	Ol + Opx + Grt	-	Cpx + Mgs	Ol + Opx + Mgs + Phl	-	-	Ol

^a Oxide average wt.% after normalization and its standard deviation (water and carbonate free basis).

of 0.12–0.22 (Table 2). A small band/shoulder at \sim 1000 cm⁻¹, in some of the spectra, is due to the presence of a daughter mica phase in these microinclusions. The shape of the water band is narrow and is similar to that of saline HDFs. The HDF-related peaks in diamond ON-DBP-332 are different, they show the IR bands of water and strong absorbance due to the daughter mica phase (central peak at \sim 1000 cm⁻¹) and quartz (1092, \sim 810 and 785 cm⁻¹); carbonate IR bands were not detected in this diamond (Fig. 2 and Supplementary Fig. 2).

The absorbance caused by pyroxene (multiple peaks in the range between 600-1150 cm⁻¹, Fig. 2 and Supplementary Fig. S2) is observed in the inner part of diamond ON-DBP-330, but the characteristic peaks are all displaced to higher wavenumbers by 5-12 cm⁻¹. No carbonate or water bands were detected in this part of the diamond, in agreement with EPMA analysis (section 3.2.1), which revealed only orthopyroxene associated with olivine microinclusions (Fig. 1), confirming that the inner zone is mostly free of HDF microinclusions. In diamond ON-DBP-335, the inner part showed strong carbonate absorbance at 1450, 881 and 750 cm⁻¹ but no significant water absorbance was detected, suggesting that the carbonate absorption is due to the presence of magnesite rather than HDF microinclusions. Peaks at 1080, 983 and 900 cm⁻¹, which are also observed in the inner part of this diamond, can be related to the presence of pyroxene. Absorbance by both a mica phase and magnesite dominate the spectrum collected in the inner part of diamond ON-DBP-336, while olivine absorbance (\sim 995, 956, 891 and 841 cm⁻¹), with no significant mica or carbonate phases, is observed in the outer regions of this diamond. The absence of water bands in the spectra collected in both zones of this diamond indicate a lack of or very small amount of HDF microinclusions in this specific diamond, in agreement with EPMA analyses (Supplementary Figs. S1 and S2, Supplementary Tables A, B).

3.2. High-density fluids and mineral microinclusions – major and trace element compositions

Three hundred and forty-seven HDF microinclusions and one hundred and ninety mineral microinclusions were analyzed in the inclusion-rich zones of the eight diamonds (Figs. 1, 3 and Supplementary Fig. S1). Seven of these diamonds (ON-DBP-330, 331, 335-339) are rich in saline HDFs; among those, five carry mineral microinclusions: olivine (Ol), orthopyroxene (Opx), clinopyroxene (Cpx), garnet (Grt), phlogopite (Phl) and magnesite (Mgs) were identified (Table 2). The microinclusions in the eighth diamond, ON-DBP-332, contains only silicic HDF. In general, all HDFs have elevated concentrations of incompatible elements relative to primitive mantle (PM), with the most incompatible elements (Cs-Pr) reaching levels of a few hundred to a few thousand times the PM values (Fig. 4). Variations between individual diamonds, and between saline and silicic HDFs, are described below. The average major element composition of the HDFs in each diamond and the minerals are presented in Tables 2 and 3, respectively, with individual microinclusion analyses tabulated in Supplementary Tables A and B; trace element analyses are presented in Supplementary Table C.

3.2.1. Mineral inclusions

Mineral microinclusions were found in five of the seven diamonds carrying saline HDFs. In backscattered-electron imaging, these inclusions appear similar in shape to HDF microinclusions and are comparable in size, but their EPMA analysis totals are on average higher (Supplementary Table B). Some microinclusions

^b Original total of oxides and Cl measured by EPMA in wt.% (before normalization).

^c CMF = CO₂/(CO₂ + H₂O) molar ratio, as calculated from the IR spectrum, using $\varepsilon_{\text{calcite}}$ 1433 cm⁻¹ = 739 and $\varepsilon_{\text{water}}$ 3420 cm⁻¹ = 87 (AU-I/mol-cm) or { $\varepsilon_{\text{water}}$ 3420 cm⁻¹ = 109} (Weiss et al., 2010). IR spectrum could not be collected for ON-DBP-331 and 339; CMF could not be calculated for ON-DBP-336 due to low water and carbonate absorbance. Therefore, for these diamonds the average saline CMF value of 0.15 {0.18} is presented. The CMF for ON-DBP-332 could not be calculated because of the lack of carbonate absorbance in its IR spectrum.

d CO₂ wt.% in HDF relative to 100% oxides, calculated according to the molar proportion of CO₃ = Mg+Fe+Ca+Ba+(Na+K-Al-Cl-Si/3)/2-5P/3-(Si-2×Ti-(Al-Si/3)×3/2) for saline HDF composition (see text for details).

^e H₂O wt.% in HDF relative to 100% oxides, calculated from the molar CO₂ value and the CO₂/(CO₂ + H₂O) ratio.

f X_{CO}, is the mole fraction of CO₂, as calculated from the HDF composition including CO₂ and H₂O wt.%, normalized to 100%.

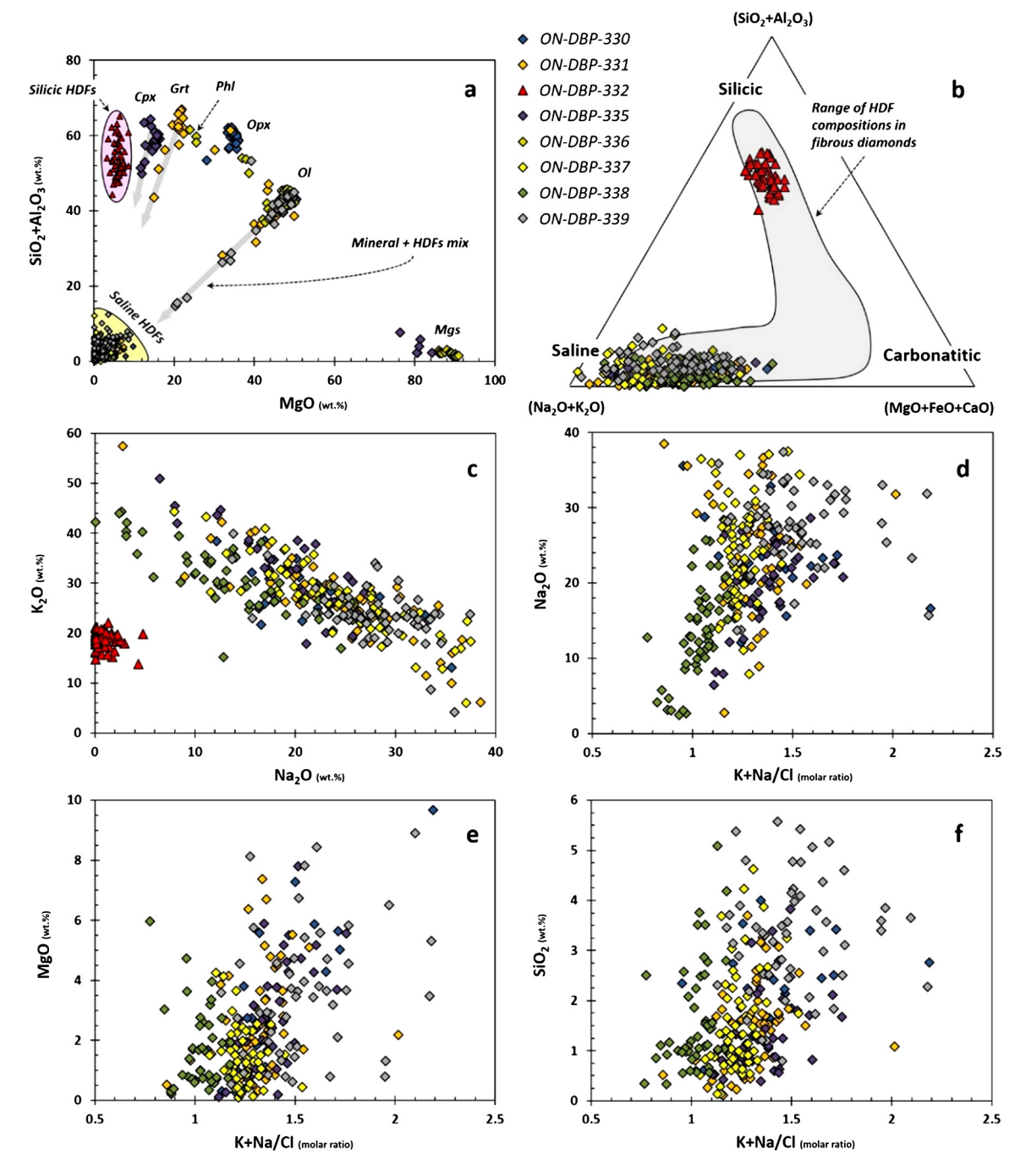


Fig. 3. Composition of mineral and HDF microinclusions in diamonds from De Beers Pool kimberlites. (a) $SiO_2 + Al_2O_3$ vs. MgO (in wt.%) showing the different mineral microinclusions (Ol – olivine, Opx – orthopyroxene, Cpx – clinopyroxene, Grt – garnet, Phl – phlogopite, Mgs – magnesite) and HDF microinclusions associated with specific De Beers Pool diamonds coded by color. The composition of some microinclusions that trapped both mineral and HDF fall along mixing lines. (b) $SiO_2 + Al_2O_3 - Na_2O + K_2O - MgO + FeO + CaO$ ternary diagram (in wt.%) showing the HDFs composition in De Beers Pool diamonds compared to the global compositional HDF chemical variation (shaded area, delineated by the average composition of 90 individual diamonds). (c) K_2O vs. Na_2O (in wt.%) showing the negative correlation between K and Na in saline HDFs in De Beers Pool diamonds (silicic HDFs are shown for comparison). (d)–(f) Na_2O , MgO and SiO_2 (in wt.%) vs. K + Na/Cl (in moles) of saline HDFs. These oxides increase (as well as CaO, Al_2O_3 and P_2O_3 to some extent) with increasing (K + Na)/Cl of the saline HDFs. (For interpretation of the colors in the figure(s), the reader is referred to the web version of this article.)

carry both mineral and HDF and the analysis represent mixture of the two (Fig. 3a). The analyzed mineral microinclusions are all of the peridotite paragenesis and always found in association with saline HDFs, but different assemblages are observed: Ol, Ol + Opx, Ol + Opx + Grt, Ol + Opx + Phl + Mgs and Cpx + Mgs (Table 2). Olivine and orthopyroxene are the most abundant mineral microinclusions in the analyzed De Beers Pool diamonds, in agreement with the predominance of these two phases in the deep lithosphere of the De Beers Pool region (Phillips et al., 2004).

and references therein). We used linear regression of the mixing lines between mineral and HDF microinclusions, which are best manifested by oxide (e.g. MgO, SiO_2) vs. Cl wt.% variation diagrams (not shown), to determine the compositions of Ol, Opx, Cpx, Grt and Mgs at Cl = 0 wt.% (Table 3). The composition of phlogopite was determined by averaging the 3 inclusions that were found in diamond ON-DBP-336. Below, the compositional variability of HDF-free mineral phases is described.

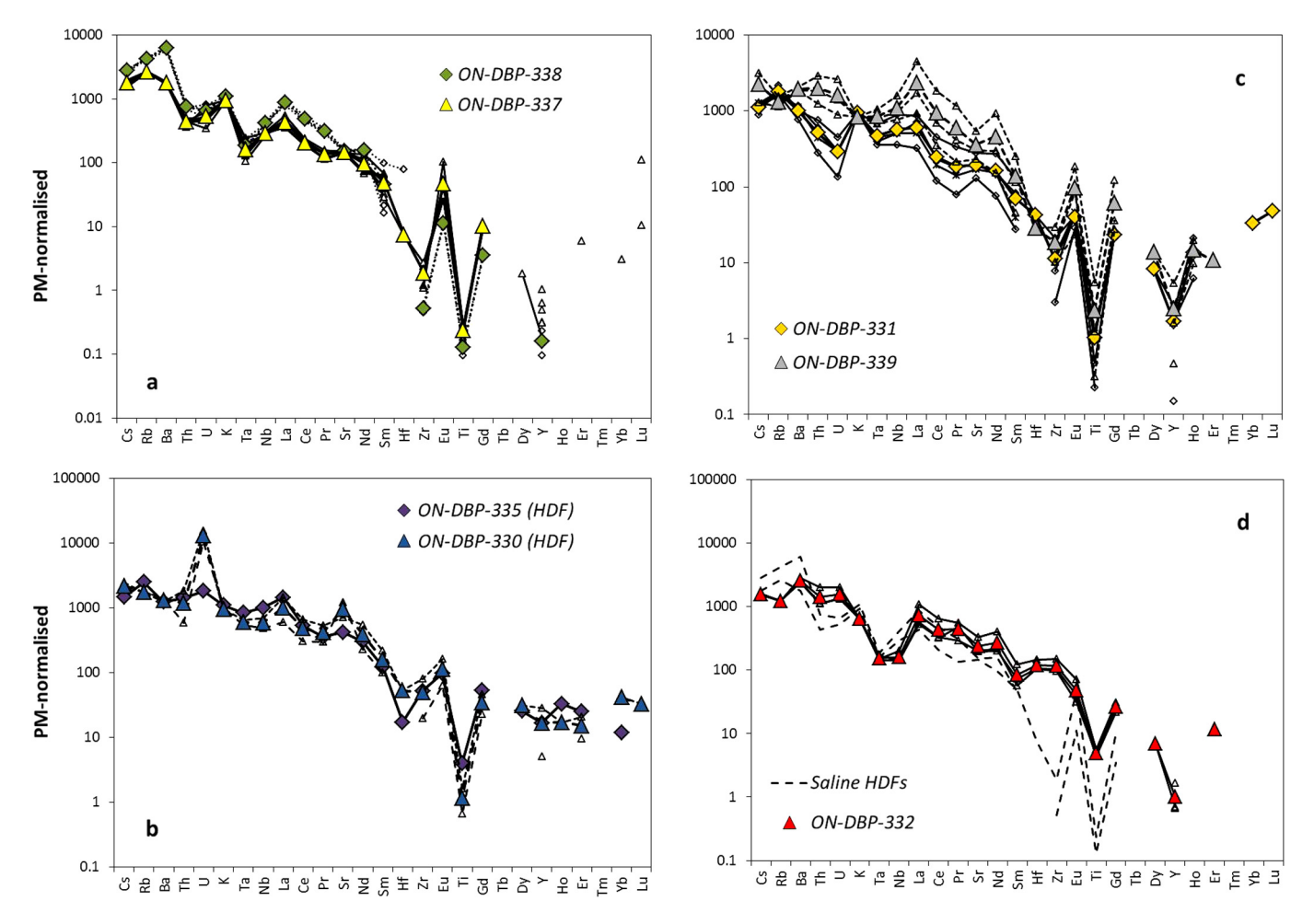


Fig. 4. Primitive-mantle-normalized incompatible-element patterns of HDFs trapped in De Beers Pool diamonds. (a) Diamonds ON-DBP-337 and 338; only HDF microinclusions were found in these diamonds. (b) Diamonds ON-DBP-330 and 335; both mineral microinclusions and fluid microinclusions were identified, but they reside in different growth zones of the diamonds. Laser ablation was conducted at the HDF-bearing outer part of these two diamonds. (c) Diamonds ON-DBP-331 and 339; mineral microinclusions and HDF microinclusions reside in the same growth zone in these diamonds. The ablated diamond volume likely contained a mixture of mineral and HDF microinclusions. (d) Diamond ON-DBP-332; only HDF microinclusions were found in this diamond. The average incompatible element pattern of saline HDF of ON-DBP-337 and 338 is plotted for comparison. In all panels (a)–(d), small symbols – individual LA-ICP-MS analyses, large symbols – HDF average composition in a single diamond. The uncertainties on the values of Yb and Lu are large and they can be regarded as qualitative only. Primitive mantle values are from McDonough and Sun (1995).

The Mg# $(100 \times Mg/(Mg + Fe))$ molar ratio of olivine microinclusions is 93.0 \pm 0.2 (1 SE on the regression intercept at Cl = 0 wt.%) while that of orthopyroxene is 93.5 ± 0.6 , typical for Kaapvaal craton mantle peridotites (e.g. Lazarov et al., 2009a). Orthopyroxene microinclusions have 0.4 ± 0.1 wt.% Cr_2O_3 , 0.9 ± 0.1 Al_2O_3 and 0.7 ± 0.2 Na₂O (one inclusion has a relatively high Na₂O value of 2.9 wt.%); in most cases TiO₂ was not detected. Clinopyroxene microinclusions were only found in the central part of diamond ON-DBP-335. They have Mg# = 93.2 ± 0.9 and Cr# ($100 \times \text{Cr/(Cr}$ + Al) molar ratio) of 47.1 \pm 2.0. Both Cr₂O₃ and Na₂O content are elevated, with values reaching up to 7.0 wt.% and 7.7 wt.%, respectively, indicating a high Na-Cr kosmochlore component endmember (up to 17 mol%). Al $_2$ O $_3$ = 3.6 \pm 0.2 wt.%, TiO $_2$ = 0.4 \pm 0.2 and K_2O show minor amounts (0.1 \pm 0.1 wt.%) in these Cpx inclusions. Garnet inclusions are Cr-pyrope with Mg# = 83.8 \pm 1.1, Cr# = 17.6 \pm 0.8, and Cr $_2O_3$ = 5.7 \pm 0.3 wt.% and CaO = 3.5 ± 0.3 wt.%. They plot in the harzburgitic depleted subcalcic garnet field of Grütter et al. (2004) and are all classified as G10 garnets, similar to many subcalcic garnet inclusions in De Beers Pool diamonds (Phillips et al., 2004). An Mg-rich phase was found in two diamonds (ON-DBP-335 and 336), having Mg# = 95.8 \pm 0.2, MgO = 88.3 \pm 0.6 wt.%, FeO = 6.9 \pm 0.2 and CaO = 1.3 \pm 0.1. SiO_2 , Al_2O_3 , Cr_2O_3 , MnO, TiO_2 , K_2O and Na_2O are all <1 wt.% each and sum up to \sim 3 wt.%. The detection of peaks at 1450, 881 and 750 cm $^{-1}$ in the FTIR spectra collected at the inner region of these two diamonds indicates that this phase is an Mg-rich carbonate phase (i.e. magnesite). Three inclusions of low-Ti phlogopite were also analyzed in diamond ON-DBP-336, having an average composition of Mg# = 95 \pm 1, 12.8 \pm 0.9 wt.% Al $_2$ O $_3$, 0.9 \pm 0.1 wt.% Cr $_2$ O $_3$ and a Si/Al and Si/(Al + Cr) (cation ratio) of 3.1 \pm 0.4 and 3.0 \pm 0.3, respectively. In addition, small amounts of 0.3 \pm 0.1 wt.% Na $_2$ O and 0.2 \pm 0.1 wt.% Cl were detected, plausibly from traces of saline HDFs within these inclusions.

The central part of diamond ON-DBP-330 contains olivine and Opx microinclusions but no HDFs (Fig. 1, Supplementary Fig. 2). We therefore analyzed this part by LA-ICP-MS, with the aim of determining the trace element composition of the peridotite host. However, most of the elements were below the limit of detection (except K, Sr, Nb, Ba, La and Ce; Supplementary Table C). Thus, we could reach no conclusions about the trace element composition or pattern of these mineral microinclusions.

3.2.2. Saline HDFs

The HDFs in all seven saline diamonds show similar chemical compositions, varying between the saline end-member and the carbonatitic end-member when projected on a $SiO_2 + Al_2O_3$, CaO + MgO + FeO and $Na_2O + K_2O$ ternary diagram (Fig. 3b). On a carbonate- and water-free basis, the average saline fluid is

 Table 3

 Mineral microinclusion composition in the De Beers Pool diamonds based on linear regression, and thermobarometry conditions of equilibration.

	Orthopyroxene	Olivine	Garnet	Clinopyroxene	Mg-rich carbonate	Phlogopite
SiO ₂ ^a	57.8 (0.7)	43.0 (0.2)	42.3 (0.6)	52.8 (0.3)	0.9 (0.2)	46.5 (2.5)
MgO	34.1 (0.5)	48.0 (0.2)	20.2 (0.2)	14.2 (0.2)	88.3 (0.6)	24.6 (0.9)
FeO	4.3 (0.4)	6.4 (0.1)	7.0 (0.6)	1.9 (0.3)	6.9 (0.2)	2.4 (0.5)
CaO	0.2 (0.1)	0.2 (0.1)	3.5 (0.3)	16.3 (0.2)	1.3 (0.1)	0.1 (0.1)
Al_2O_3	0.9 (0.1)	0.6 (0.1)	17.9 (0.5)	3.6 (0.2)	0.9 (0.1)	12.8 (0.9)
Na ₂ O	0.7 (0.2)	0.0 (0.1)	0.3 (0.3)	4.9 (0.3)	0.0 (0.1)	0.3 (0.1)
K ₂ O	0.1 (0.1)	0.4 (0.1)	1.2 (0.5)	0.1 (0.1)	0.1 (0.1)	11.2 (0.8)
TiO ₂	0.1 (0.1)	0.1 (0.0)	0.3 (0.1)	0.4 (0.2)	0.2 (0.1)	0.0 (0.0)
Cr_2O_3	0.4 (0.1)	0.2 (0.1)	5.7 (0.3)	4.8 (0.3)	0.4 (0.1)	0.9 (0.1)
MnO	0.5 (0.3)	0.3 (0.0)	1.1 (0.5)	0.4 (0.1)	0.6 (0.1)	0.1 (0.1)
Total ^c	99.1	99.1	99.4	99.5	99.5	98.9
Mg# ^b	93.5 (0.6)	93.0 (0.2)	83.8 (1.1)	93.2 (0.9)	95.8 (0.2)	95 (1)

Temperature (°C) calculated with preset pressured

	3 GPa	4 GPa	5 GPa	6 GPa	7 GPa	8 GPa
T [RV]	925	1003	1081	1158	1236	1314
T [OW]	788	841	889	933	972	1007
T [NG]	822	922	1022	1122	1222	1321
T [HR]	875	932	990	1047	1105	1163
T [BK]	774	833	892	951	1010	1069

Pressure (GPa) calculated with preset temperature

	750°C	900°C	1050°C	1200°C	1300°C	1400°C
P [NG]	4.8	5.8	6.9	8.0	8.7	9.4
P [MC]	2.7	3.6	4.6	5.5	6.1	6.8
P [NT]	4.7	5.4	6.1	6.8	7.2	7.7

- ^a Oxide wt.% composition (at Cl = 0 wt.%) and its standard error, as determined using linear regression to the mixing lines between mineral and HDF microinclusions in oxides vs. Cl variation spaces.
- b Mg# = $100 \times Mg/(Mg + Fe)$ molar ratio.
- $^{\rm c}$ Total = the sum of the different oxide compositions at Cl = 0 wt.%.
- d Temperature was calculated using the garnet-clinopyroxene Mg-Fe exchange thermometer of Ravana Krogh (2000) [RV], olivine-garnet Mg-Fe exchange thermometer of O'Neill and Wood (1979) [OW] and the garnet-orthopyroxene Mg-Fe exchange thermometers of Harley (1984) [HR], Brey and Köhler (1990) [BK] and Nimis and Grutter (2010) [NG].
- e Pressure was calculated using the Al in orthopyroxene barometer of MacGregor (1974) [MC], Cr in clinopyroxene barometer of Nimis and Taylor (2000) [NT] and the garnet–orthopyroxene barometer of Nickel and Green (1985) [NG] (with modified Mg-Tschermaks according to Taylor, 1998).

primarily rich in Cl (35.7 \pm 2.2 (1 σ for the 7 diamond averages) wt.%), K_2O (27.1 \pm 3.5 wt.%) and Na_2O (22.3 \pm 4.7 wt.%). Other major oxides make up about 15 wt.% altogether: SiO₂ = 2.2 ± 1.2 , CaO = 8.5 ± 1.6 , MgO = 2.7 ± 1.3 , FeO = 5.7 ± 1.3 1.4, BaO = 1.5 \pm 1.3, Al₂O₃ = 1.0 \pm 0.4, P₂O₅ = 0.9 \pm 0.5 and $TiO_2 = 0.5 \pm 0.3$ wt.% (as these saline fluids carry Cl⁻ as a major anion, the total Cl + oxides sum up to >100% due to excess calculated oxygen). The molar proportions of carbonate in the HDF can be estimated assuming cations with positive charge in the fluid are balanced by either carbonate, chloride, phosphate or silicate ions, we further assume that the silicate phase is mica and obtain (all in molar proportions): CO₃ = Mg+ $Fe+Ca+Ba+(Na+K-Cl-Si/3)/2-5P/3-(Si-2\times Ti-(Al-Si/3)\times 3/2).$ The term with the first parentheses accounts for the binding of Na and K in salt and in mica, next term accounts for Ca in apatite and the last one for Mg and Fe in mica. Once the CO2 is calculated, the water content is determined based on the FTIR CMF ratio (Table 2). When both water and carbonate are included and the total is re-normalized to 1 kg of water (55.5 mol), the saline HDFs have an average molal proportions of: Si_{0.9}Ti_{0.1}Al_{0.4} $Fe_{1.8}Mg_{1.6}Ca_{3.5}Ba_{0.2}Na_{16.6}K_{13.3}P_{0.3}Cl_{23.2}(CO_2)_{9.4}(H_2O)_{55.5}$. Assuming that the main components of the saline HDFs are water, chlorides, carbonates, phosphates and silicates, chlorides make up 42% by weight, carbonates - 27%, silicates - 3%, phosphates - 1% and water make up 27% of the HDFs.

The major element composition of the saline HDFs show intraand inter-diamond relationships. In all diamonds K_2O and Na_2O show a negative correlation (Fig. 3c), $K_2O + Na_2O$ exhibit a clear positive correlation with Cl and the Cl/(Cl + K + Na) ratio increases with increasing K/(K + Na). MgO correlate negatively with Cl. as do FeO and CaO but with a wider scatter. In addition. in diamond ON-DBP-335 CaO and P2O5 correlates positively and in ON-DBP-330 SiO2 correlates negatively with Cl. The inner and outer zones of diamond ON-DBP-337 (Supplementary Fig. S1) show slightly different saline compositions, that is, HDF microinclusions in the outer zone have on average higher MgO, FeO, CaO, BaO and K_2O , and lower Na_2O and Cl. The molar (K + Na)/Cl ratio in diamonds ON-DBP-338 and 337 varies between 1.01 \pm 0.09 (1 σ) and 1.24 ± 0.09 , respectively, while it increases up to (K + Na)/Cl =1.33 \pm 0.12, 1.37 \pm 0.17 and 1.55 \pm 0.31 in diamonds ON-DBP-336, 335 and 339, respectively. These variations to higher (K + Na)/Clvalues correlate with a general increase of MgO, SiO2 and Na2O of the HDF microinclusions in the different diamonds (Fig. 3d-f). In addition, CaO, Al₂O₃ and P₂O₃ also increase to some extent with increasing (K + Na)/Cl (not shown). Consequently the calculated CO_2 contents of the HDFs increase by 32%, from $CO_2 = 9.1$ wt.% in diamond ON-DBP-338 to CO₂ = 12.0 wt.% in diamond ON-DBP-339 (Table 2). This increase in CO₂ correlates with increase in (K + Na)/Cl and with increase in the Mg# of the HDFs.

The trace element compositions of the two diamonds where only saline HDF microinclusions were found (ON-DBP-337 and 338) are very similar (Fig. 4a). They have high alkalis (K, Rb and Cs), Ba and LREEs compared to Th, U, Nb and Ta levels, and are characterized by conspicuous Ti, Zr, Hf and Y negative anomalies. Variations from these patterns are observed in diamonds where HDF microinclusions reside within an outer growth zone, apparently separated from the mineral microinclusions in an inner part (i.e. diamond ON-DBP-330 and 335), as well as in diamonds containing a mixture of HDF and mineral microinclusions (ON-DBP-331 and 339) (Fig. 1, Fig. 4 and Supplementary Fig. S1). In these

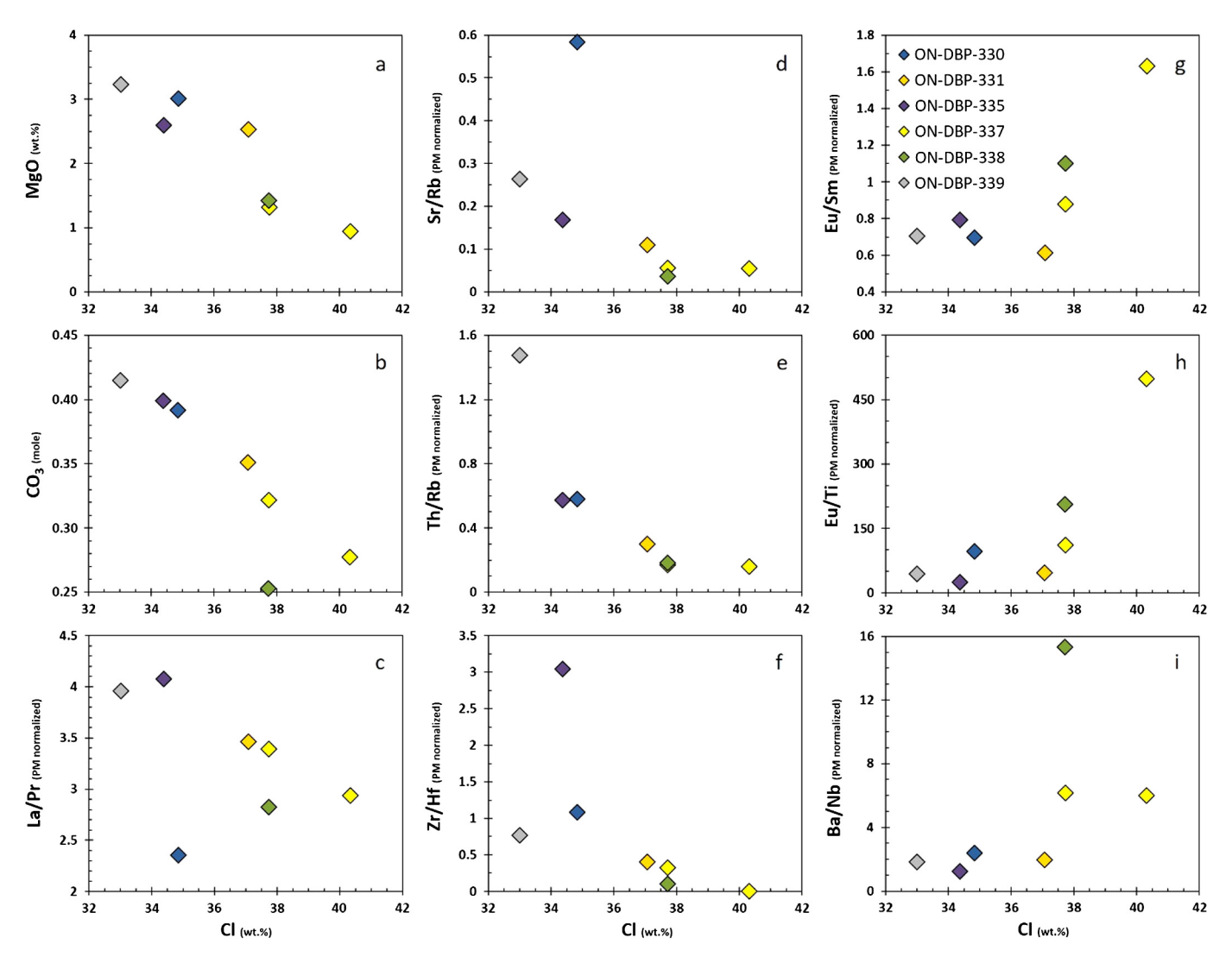


Fig. 5. Relationships between trace element ratios, MgO (in wt.%), the calculated molar carbonate content and the Cl content (in wt.%) in saline HDFs in De Beers Pool diamonds. The MgO and carbonate content which represent the carbonatitic end-member component in the saline HDFs correlate negatively with increasing Cl (a)–(b). With increasing carbonatitic component, La/Pr ratio increases and Eu/Sm and Ba/Nb ratios decrease in the saline HDF, while Sr/Rb, Th/Rb and Zr/Hf ratios increase and Eu/Ti ratio decrease, due to higher Sr, Th, Zr and Ti concentrations (c)–(i).

diamonds the differences in enrichment between the most incompatible elements (Th, U, Nb and Ta) and the alkalis, Ba and LREEs are reduced. The negative anomalies of Ti, Zr, Hf and Y are also smaller. These compositional changes are manifested as correlative variations between trace element ratios and the average amount of Cl and MgO (and carbonate), which correlate negatively in the saline HDFs (Fig. 5). In general, with decreasing Cl and increasing MgO, the La/Pr ratio increases and Eu/Sm and Ba/Nb ratios decrease; Sr/Rb, Th/Rb and Zr/Hf ratios increase and Eu/Ti ratio decrease, due to higher amounts of Sr, Th, Zr and Ti. There are some outliers for the different trace element ratios, but these do not change the general trends observed in most diamonds.

3.2.3. Silicic HDFs

The HDF microinclusions in diamond ON-DBP-332 have well defined chemical composition, close to the silicic end-member HDF (Fig. 3b). On a carbonate- and water-free basis, its average composition is primarily rich in SiO₂ (48 \pm 4.5 (1 σ) wt.%) and K₂O (18.5 \pm 1.8 wt.%). Other major oxides make up about 35 wt.% altogether (Table 2). SiO₂ exhibits a negative correlation with CaO and P₂O₅. Carbonate absorbance was not detected by FTIR analyses in this diamond (Supplementary Fig. S2) and thus, the CMF ratio of the

included HDFs could not be determined, nor could the molar proportions of water and carbonate be estimated.

The trace element compositions of the silicic HDFs are comparable to the saline fluids in diamond ON-DBP-337 and 338, however a few key differences exist (Fig. 4d). Normalized to primitive mantle values, Th, U and Ba in the silicic fluids are similarly enriched and are elevated compared to the alkalis (K, Rb and Cs). Zr and Hf show positive anomalies compared to elements of similar compatibility during mantle melting, in contrast to the saline HDFs, while the negative anomaly of Ti is relatively small. Ta and Nb show comparable depletion compared to LREEs in both silicic and saline compositions.

3.3. Thermometry, barometry and oxygen fugacity

Temperature conditions during saline metasomatism and fluid-rich diamond formation were calculated using the composition of HDF-free mineral microinclusions in the saline HDF-bearing diamonds (Table 3). Equilibrium temperatures were determined with preset pressures between 3–8 GPa using the two-pyroxene thermometer (Brey and Köhler, 1990) and the Mg–Fe exchange thermometers between garnet–clinopyroxene (Krogh, 2000), garnet–olivine (O'Neill and Wood, 1979) and garnet–orthopyroxene (Harley,

1984; Nimis and Grütter, 2010). Pressure conditions were calculated using preset temperatures between 750–1400 °C and various barometers: Al in orthopyroxene (Macgregor, 1974), Cr in clinopyroxene (Nimis and Taylor, 2000) and the garnet–orthopyroxene barometer (Nickel and Green, 1985) with modified Mg-Tschermaks according to (Taylor, 1998). Results are presented in Table 3.

Below the graphite-diamond stability line the different thermometers and barometers define a slanted rhomb shape (Fig. 6a), varying over $\sim 500\,^{\circ}\text{C}$ between 4–8 GPa, as the possible temperature conditions for saline metasomatism and the formation of the De Beers Pool diamonds that carry saline HDF microinclusions. However, at any given pressure the variation in temperature is \sim 200 °C, so that, for example at 5 GPa, the possible range of temperature is between 875-1080°C and at 6 GPa lies between 930–1155 °C. Mineral microinclusions of both peridotite and eclogite lithologies in diamonds carrying saline HDFs from the neighboring Koffiefontein kimberlite suggest similar temperature and pressure conditions (Izraeli et al., 2004). In addition, the saline HDFs-bearing diamonds from the two localities (De Beers Pool and Koffiefontein) carry nitrogen almost exclusively in A-centers (Table 1 and Supplementary Fig. S2; Izraeli et al., 2004), indicating formation temperatures of less than 1200 °C (Taylor et al., 1990).

Oxygen fugacities (fO_2) for the saline HDFs were calculated using the calibration of Stagno and Frost (2010). This calibration assumes ideal system in which the activity of CO2 in the melt is equal to the mole fraction of CO_2 (X_{CO_2}) in the melt, and it closely reproduces experimental results for melt fO2 in a Cabearing peridotite system between 2.5 and 11 GPa. Dilution of carbonate (lower X_{CO_2}) decrease the carbonate activity, and determine the maximum fO_2 stability of carbonate-bearing melts relative to the EMOG/D buffer (Fig. 6b). Using the X_{CO_2} of the saline HDFs (Table 2) over the range of temperature and pressure presented in Fig. 6a, we calculated a range of log fO2 relative to the FMQ buffer between $\Delta \log f O_{2(FMO)}$ of -2.57 and -1.45 (variation at a given pressure is $<0.37 \Delta \log \text{ units}$; Fig. 6b). These results indicate that the fO_2 conditions during saline metasomatism were lower by only 0.6-0.2 $\Delta \log$ units compared to the EMOG/D reaction curve at 5 GPa and by $0.7-0.5 \Delta \log \text{ units}$ at 7 GPa (Fig. 6b).

4. Discussion

4.1. High-density fluids (HDFs) in De Beers Pool diamonds – mantle source, lithospheric host rock and fluid evolution

The chemical compositions of HDF microinclusions in fluidrich diamonds reflect the various mantle sources of deep mantle metasomatic fluids, which impact the lithosphere and form diamonds. Investigations of the nature of HDFs trapped in fluid-rich diamonds have revealed four compositional end-members globally: saline HDFs that carry mostly K, Na, Cl and water with some carbonates and silicates; high-Mg carbonatitic HDFs characterized by high MgO and carbonate, and low silica, alumina and water; and a continuous array between silicic and low-Mg carbonatitic HDFs with varying amounts of silicates, carbonates and water (e.g. Klein-BenDavid et al., 2009; Navon et al., 1988; Skuzovatov et al., 2016; Smith et al., 2012; Tomlinson et al., 2006; Weiss et al., 2009). Within this framework, Weiss et al. (2015) reported the first conclusive trace-element (i.e. strong and correlative positive anomalies of Eu and Sr) and Sr isotope evidence for seawater-altered subducting slabs as the source of saline HDFs in a set of diamonds from the Northwest Territories, Canada. Saline HDFs in the analyzed De Beers Pool diamonds do not have pronounced positive anomalies of Eu and Sr. In most cases they show small positive or no anomalies for Sr, and $(Eu/Sm)_{PM} < 1$ (Figs. 4, 5g), and give no indication of derivation from recycled oceanic crust. However, the thermal conditions of saline metasomatism in

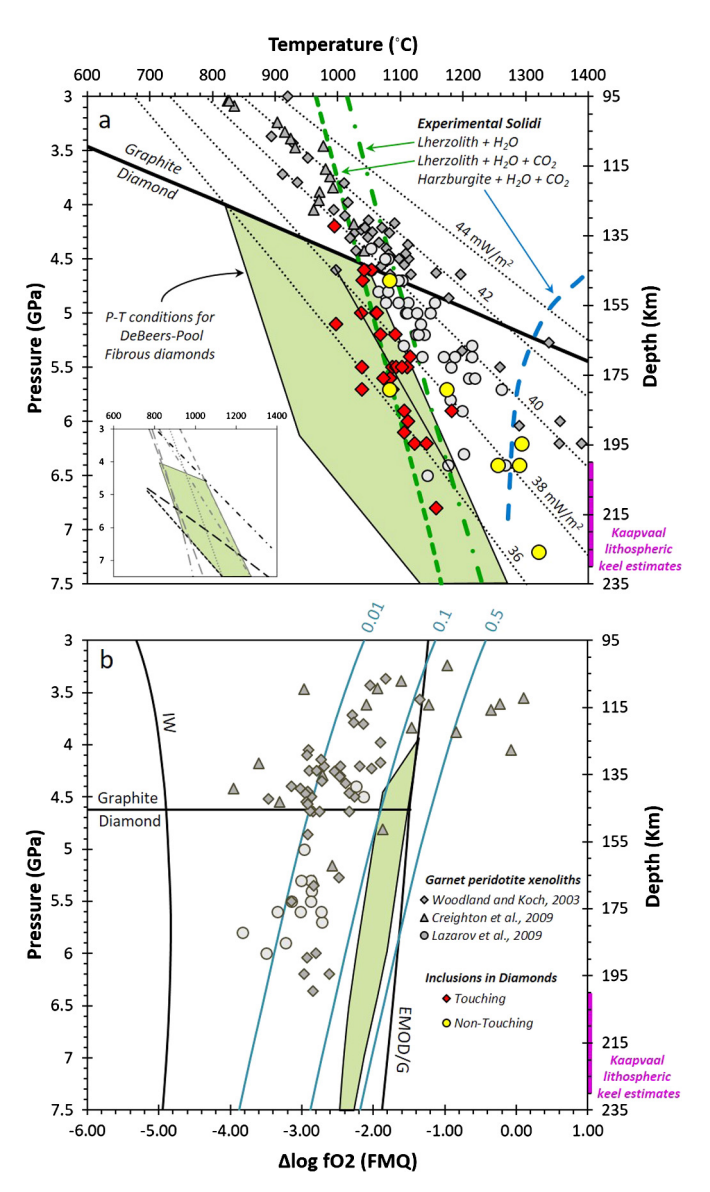


Fig. 6. Temperature-pressure- fO_2 conditions of peridotitic diamond inclusions and xenoliths from the southwestern Kaapvaal craton. (a) The green area represents the possible P-T conditions of saline metasomatism as recorded by non-touching mineral microinclusions in saline HDF-bearing diamonds from De Beers Pool (this study), the inset shows the different thermometers and barometers which were used to define these conditions (see text for additional information). Also shown are P-T conditions of mineral inclusions in monocrystalline diamonds (touching pairs red diamonds, non-touching – yellow circles; Phillips et al., 2004); 36–44 mW/m² continental geotherms (black dotted lines; Hasterok and Chapman, 2011); graphitediamond transition (black solid line; Day, 2012); the solidus for lherzolite + H₂O + CO₂ and lherzolite + H₂O (green dashed and dotted-dashed lines; Wyllie and Ryabchikov, 2000), and the solidus for harzburgite $+ H_2O + CO_2$ (blue dashed line; Wyllie, 1987). (b) fO2 variations of saline HDFs as a function of pressure (green area), fO_2 was calculated using the possible P-T conditions of mineral microinclusions in (a), the composition of HDFs in the different diamonds (Table 2) and the calibration of Stagno and Frost (2010). Also shown are the iron-wüstite buffer reaction (IW; Ballhaus et al., 1991), the graphite-diamond transition, the enstatite + magnesite = olivine + graphite/diamond reaction (EMOG/EMOD; Holland and Powell, 2011), and the fO_2 stability of carbonate-bearing melts (blue lines with molar fraction of CO_2 on top; Stagno and Frost, 2010). Xenoliths P-T data (gray diamonds, triangles and circles) are from Woodland and Koch (2003), Creighton et al. (2009) and Lazarov et al. (2009b): their fO_2 values are calculated based on Stagno et al. (2013). The depth of the Kaapvaal lithospheric keel is estimated based on Rayleigh wave tomography (Chevrot and Zhao, 2007), seismic anisotropy (Fouch and Rondenay, 2006) and electrical-conductivity measurements (Miensopust et al., 2006).

the Kaapvaal SCLM, as determined by geothermobarometry of non-touching mineral microinclusions in the De Beers Pool diamonds, reflect the interaction of low temperature saline HDFs with lithospheric rocks (Fig. 6a; see section 4.3 below for details and discussion). In addition, the redox states of these saline HDFs are higher compared to the local SCLM, and approach the EMOD reaction curve (Fig. 6b). These two lines of evidence indicate that the saline metasomatic agent that altered the southwestern Kaapvaal SCLM were 'cold and oxidized' in nature, and could not originate from the ambient lithosphere nor from the underlying 'hotter' asthenosphere. We therefore suggest that the saline HDFs in De Beers Pool diamonds are linked to a subducting slab, feasibly through a relationship to early Mesozoic flat-plate subduction under the southwestern margin of Gondwanaland (Lock, 1980).

Weiss et al. (2015) showed a chemical evolutionary trend indicating that silicic HDFs in diamonds from the Northwest Territories formed through fluid-rock interaction of parental saline fluids with eclogitic lithologies in the lithospheric mantle. In the case of the De Beers Pool diamonds reported here, we preclude a direct relationship between the saline and silicic HDFs based on the different states of nitrogen aggregation of their host diamonds (Fig. 2 and Supplementary Fig. S2), which translate to differences in time of metasomatism and diamond formation (Section 4.2). In addition, the lack of mineral microinclusions in diamond ON-DBP-332 does not allow a direct link between the silicic HDFs in this diamond and an eclogite. However, the high silica content of these HDFs (48 \pm 4.5 wt.%; Table 2) is consistent with the composition of near-solidus silicic melts/fluids in equilibrium with eclogite (Hammouda, 2003; Kessel et al., 2005), rather than peridotite (e.g. Kessel et al., 2015). This compositional HDF-lithology relationship is also supported by the finding of omphacitic pyroxene in association with silicic-to-low Mg carbonatitic HDFs in diamonds from Canada, Guinea and Siberia (Klein-BenDavid et al., 2009; Tomlinson et al., 2006; Weiss et al., 2009, 2015).

Saline HDFs in De Beers Pool diamonds invaded lithospheric peridotite, based on their microinclusions of olivine, orthopyroxene and Cr-pyrope. Fluid-rock interaction during percolation is reflected by moderate increase of SiO2, MgO and Na2O and decreases of Cl in the saline HDFs, along with higher La/Pr, Sr/Rb, Th/Rb and Zr/Hf ratios and lower Eu/Sm, Eu/Ti and Ba/Nb ratios, respectively (Fig. 3c-f, Fig. 5). The appearance of peridotite microinclusions associated with magnesite, phlogopite and kosmochlorbearing diopside in the inner part of diamonds ON-DBP-335 and ON-DBP-336 (Supplementary Fig. S1) indicates that the De Beers Pool lithosphere was previously altered, likely by enriched Nabearing carbonatitic melt (Ikehata and Arai, 2004). The possible P-T conditions for saline metasomatism intersect the lherzolite + H₂O \pm CO₂ solidus (Fig. 6a), which potentially leads to melting and formation of high-Mg carbonatitic HDFs (Weiss et al., 2009, 2015). However, high-Mg carbonatite compositions were not found as HDF microinclusions in De Beers Pool diamonds that were analyzed in the present study, nor in fluid-rich diamonds from the neighboring Koffiefontein kimberlite (Izraeli et al., 2001). Mineral inclusions in monocrystalline diamonds from De Beers Pool, Koffiefontein and Jagersfontein (Rickard et al., 1989; Phillips et al., 2004; Tappert et al., 2005) indicate that the local peridotite SCLM is dominated by harzburgite lithology, and the P-T conditions of saline metasomatism does not intersect the harzburgite $+ H_2O + CO_2$ solidus (Fig. 6a). We therefore suggest that the refractory nature of harzburgite in the southwestern Kaapvaal SCLM, although containing carbonate metasomes, prevented melting and formation of high-Mg carbonatite during saline metasomatism, and that diamonds could form by isochemical precipitation (Stachel and Luth, 2015; Sverjensky and Huang, 2015) or redox processes (Jacob et al., 2014) due to strong disequilibrium between saline HDFs and the local SCLM (Fig. 6).

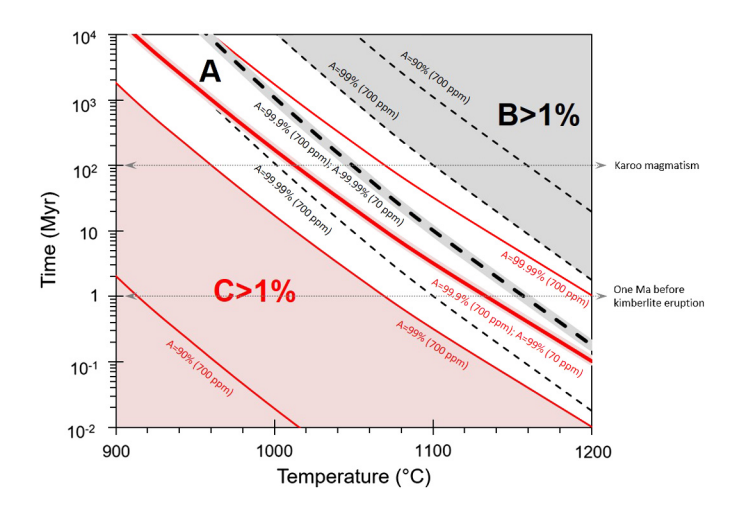


Fig. 7. The aggregation of nitrogen from C-centers (single nitrogen atom) to Acenters (paired nitrogen atoms), and from A-centers to B-centers (aggregates of four nitrogen atoms) as a function of time and temperature, using the calibrations of Taylor et al. (1990, 1996). The proportions of nitrogen in A-centers increase with time and temperature as single nitrogen atoms combine to nitrogen pairs (solid red contours), and decrease as nitrogen pairs aggregate to form larger aggregates of four atoms (dashed black contours). Diamonds showing 'pure' Type IaA spectrum contain unresolved B-centers or C-centers, that account to less than 1% of the total nitrogen (middle white field). The low-aggregated nature of nitrogen in the De Beers Pool diamonds suggest the timing of their formation is younger than the Karoo flood basalt volcanism at 180 \pm 5 Ma, which involved a major increase in the temperature of the South African lithosphere. At 1150 °C and <0.1% of both B- and C-centers (Acenters >99.9%), the mantle residence time of the saline HDF-bearing diamonds, with nitrogen concentrations varying between 70-700 ppm, is only a few million years before kimberlite eruption. At 1000 °C the estimated residence time for these diamonds is longer (on the order of hundreds of millions of years), but if we allow a higher concentration of C-centers (up to 1%) with less than 0.1% of B-centers, shorter residence times of the order of tens of millions of years are also possible. If, indeed, the diamonds carrying the saline HDFs resided only a few millions to tens of millions of years in the mantle, the presence of more than 99% of the nitrogen in A centers indicates residence temperatures of 1000-1150 °C, in agreement with the P-T conditions indicated by the mineral microinclusions (Fig. 6).

4.2. Timing of metasomatism and fluid-rich diamond formation

The overall absence of large silicate and sulfide inclusions in fluid-rich diamonds precludes absolute age determination, i.e. the age of the metasomatic event in which they formed. Therefore, temporal information is commonly drawn from the kinetics of nitrogen aggregation in the diamond lattice, which is a function of the diamond 'mantle residence time' (i.e. from diamond formation until it ascended with the kimberlite), the diamond 'mantle residence temperature' (average temperature over mantle residence time) and the diamond nitrogen concentration (Evans, 1992; Taylor et al., 1990, 1996).

The saline HDF-bearing diamonds from De Beers Pool kimberlites show pure Type IaA spectra (Supplementary Fig. S2 and Table 1), with no detectable signals of B-centers or C-centers. Using the kinetics of C- to A-centers and A- to B-centers (Taylor et al., 1990, 1996) the diamond 'mantle residence time' can be constrained (Navon, 1999). However, it is hard to resolve the presence of nitrogen centers (C, A or B) when they account for less than 1% of the total nitrogen content. Fig. 7 shows that at the conditions where 99.9% of the nitrogen reside in A-centers, both C- and B-centers are present at levels of <0.1%. Diamonds that carry 70-700 ppm nitrogen and show pure Type IaA spectrum (Acenters >99.9%) can reside only a few million years at 1150°C, but this time grows up to 1000s of Myr at 1000°C and to longer than the age of the earth at 900 °C (see also Table 1). Age determinations of Type IaA diamonds should therefore be viewed with caution.

In the case of the saline HDF-bearing diamonds from De Beers Pool kimberlites, several lines of evidence suggest their formation in proximity to the kimberlitic eruptions, 1) The compositional similarities of the trapped HDFs in these diamonds suggest they all formed during a single metasomatic event and over a short period in time. 2) The temperature of equilibration of touching inclusion pairs in monocrystalline diamonds from De Beers Pool, which allowed chemical exchange and equilibration at depth, represent the final mantle ambient temperatures in which diamonds resided (Phillips et al., 2004); they overlap with possible saline metasomatism conditions between 1000-1150 °C and 4.5-7 GPa (Fig. 6a). 3) The Karoo magmatism involved a major increase in the temperature of the South African lithosphere (Bell et al., 2003; Janney et al., 2010), followed by slow adjustment of temperature and low cooling rates (Bedini et al., 2004; Michaut and Jaupart, 2007). These arguments, together with the low-aggregated nature of nitrogen in the saline HDF-bearing diamonds, suggest the timing of their formation is younger than the Karoo flood basalt volcanism at 180 \pm 5 Ma (Jourdan et al., 2007). At 1150 °C and <0.1% of both B- and C-centers, the mantle residence time of the saline HDFbearing diamonds is only a few million years (Fig. 7). At 1000 °C the estimated residence time is longer (on the order of hundreds of millions of years), but if we allow a higher concentration of C-centers (up to 1%) with less than 0.1% of B-centers, shorter residence times of the order of tens of millions of years are also possible.

Diamond ON-DBP-332, carrying silicic HDFs, is a Type IaAB diamond with 25% B-centers (Fig. 2). Two scenarios can explain the differences in nitrogen aggregation and HDF compositions between ON-DBP-332 and the saline HDF-bearing diamonds from De Beers Pool kimberlites. 1) Assuming all fluid-rich diamonds from De Beers Pool formed over a similar timeframe before kimberlite emplacement, then the nitrogen aggregation differences can be explained by a 100-150 °C variation in the diamonds' mantle residence temperatures, which translates to a pressure difference of \sim 1 GPa along the 36–38 mW/m² geotherms (Fig. 6a). While not unreasonable, this scenario restricts diamond formation by saline metasomatism to shallower depth compared to diamond formation by silicic metasomatism. 2) Considering the metasomatic events taking place over a short period of time (as mentioned above), the nitrogen aggregated nature of diamond ON-DBP-332 restricts its formation to an earlier and different metasomatic event than the one responsible for the formation of saline HDF-bearing diamonds. We prefer this scenario as it provides a simple explanation for both the nitrogen and HDF compositional variations within the De Beers Pool fluid-rich diamonds, and allows their formation at similar lithospheric depth. The lack of mineral microinclusions in diamond ON-DBP-332 offers no temperature constraints on its formation. Therefore, the timing of 'earlier' silicic metasomatism, based on nitrogen aggregation, is hard to evaluate. However considering a residence temperature of 1170–1180 °C to explain the aggregated nature of nitrogen in this diamond, and the accompanying silicic affinity of HDF microinclusions, a relation to silica-rich melts that invaded the southwestern Kaapvaal SCLM during the Karoo magmatism at ca. 180 Ma (Giuliani et al., 2014; Rehfeldt et al., 2008) is plausible.

4.3. Thermal and oxygen fugacity variations during Mesozoic metasomatism at the southwestern Kaapvaal lithosphere

Thermobarometry and oxythermobarometry of xenoliths and xenocrysts carried by kimberlites allow both the reconstruction of palaeogeotherms (e.g. Griffin et al., 2003; Rudnick, 1999) and oxidation profiles with depth (e.g. Frost and McCammon, 2008; Woodland and Koch, 2003), thus providing direct information on the thermal structure and redox state of the lithosphere of different geographical provenances and at different points in time.

Garnet peridotite xenoliths from Cretaceous Group I kimberlites at the southwestern Kaapvaal craton record temperatures that fall predominantly along a conductive continental geotherm of 40-42 mW/m² (Fig. 6a). In comparison, xenoliths from the neighboring Finsch kimberlite, a Group II kimberlite that erupted \sim 30 Ma prior to Group I kimberlites and is located \sim 130 km to the northwest, record lower temperatures that plot mainly along a geotherm of 38–40 mW/m². Similarly, garnet xenocrysts carried by Cretaceous Group I kimberlites record higher lithospheric temperatures compared to xenocrysts from Group II kimberlites (Griffin et al., 2003; Kobussen et al., 2009). These temperature differences between lithospheric samples closely related in space and time were argued as indicating a local perturbation from a 'cratoniclike' steady state condition, represented by the P-T gradient of xenoliths from Finsch, to higher thermal gradients, as observed by xenoliths from Group I kimberlites, due to Cretaceous metasomatism and volcanism (Bell et al., 2003; Griffin et al., 2003; Kobussen et al., 2009; Lazarov et al., 2009b). The xenoliths reveal a general decrease in fO2 with depth (Fig. 6b), which results principally from the increase of $Fe^{3+}/\sum Fe$ in garnet with increasing pressure (Gudmundsson and Wood, 1995; Woodland and Oneill, 1993). On the other hand, Luth and Stachel (2014) modeled the oxidizing effect of fluid-rock interaction on mantle peridotite, and concluded that ppm levels of fluid can potentially shift the fO_2 signature of lithospheric peridotite from very reduced (i.e. the iron-wüstite buffer reaction, IW) to oxidized (EMOD/G) conditions. Consequently, it was suggested that the fO_2 profile of xenoliths from the Kaapvaal Craton (Fig. 6b) merely reflects the redox state of the last metasomatic interaction (Luth and Stachel, 2014; Stachel and Luth, 2015).

The geothermobarometry of non-touching mineral microinclusions in the saline HDF-bearing diamonds from De Beers Pool (Fig. 6a) constrain the possible thermal conditions during saline metasomatism, which preceded the Cretaceous Group I kimberlite event. These conditions overlap with equilibration temperatures of touching inclusion pairs in monocrystalline diamonds from De Beers Pool, and on average are altogether lower by 150-250°C compared to the observed P-T gradient of peridotite xenoliths from both Group II and Group I kimberlites. A significant temperature difference persists, even when a possible underestimation of ~60°C is taken into account, due to differences between the garnet-orthopyroxene thermometer (used for the inclusions) and the two-pyroxene thermometer (used for the xenoliths) (Brey and Köhler, 1990; Harley, 1984). If mantle-derived xenoliths from the southwestern Kaapvaal lithosphere record a snapshot of thermal advection during the last event of metasomatism and/or kimberlite eruption (e.g. Bell et al., 2003), then the P-T conditions of nontouching mineral microinclusions in fluid-rich diamonds, touching inclusion pairs in monocrystalline diamonds, and from the xenoliths, should all plot along a similar P-T gradient; however, this is not the case. To reconcile the temperature discrepancy between inclusions in diamonds and xenoliths, we suggest that xenoliths did not equilibrate during the last metasomatic event or kimberlite eruption, and that the P-T gradients they record represent older lithospheric conditions. Moreover, we observe a gap between the fO_2 conditions of saline HDFs and peridotitic xenoliths (Fig. 6b). It implies that the redox states recorded by peridotitic xenoliths from the southwestern Kaapvaal lithosphere, similar to their P-T gradients, do not represent the interaction with saline HDFs during the last metasomatic event, but rather a reflection of the pre-existing lithospheric fO_2 conditions.

Combining the xenolith data with results for HDF microinclusions and mineral inclusions in diamonds provides a better constraint for the thermal and redox history of the southwestern Kaapvaal lithosphere with respect to Mesozoic metasomatism and volcanism. The last major thermal event in the Kaapvaal craton is

the Karoo magmatism at ca. 180 Ma, expressed by extensive volcanism of flood basalts and related giant sills and dike swarms over an area of more than 3×10^6 km², which includes the entire southern African region (Jourdan et al., 2007). The P-T gradient of xenoliths from the southwestern Kaapvaal lithosphere, along a continental geotherm of 40 ± 2 mW/m² (Fig. 6a), and their redox state (Fig. 6b), is likely a remnant of this event. Modal metasomatism in dunite and wehrlite xenoliths from De Beers Pool (Rehfeldt et al., 2008), U-Pb ages of LIMA mineral and zircon (170-190 Ma) in associated phlogopite and clinopyroxene-rich peridotite xenoliths (Giuliani et al., 2014), as well as the apparent relation between the formation of diamond ON-DBP-332 and the Karoo magmatism (discussed above), all suggest that the related metasomatism involved silicic melts. The other two volcanic events at the southwestern Kaapvaal craton are the eruption of Group II and Group I kimberlites at 125 \pm 10 Ma and 85 \pm 5 Ma (Field et al., 2008 and references therein), respectively. Compared to the Karoo magmatism, kimberlitic eruptions are local and of small volume, and likely had limited thermal influence on the lithosphere. This suggestion is supported by the non-touching mineral inclusions in the fluid-rich diamonds, formed close in time to the kimberlite eruption, and touching inclusions in monocrystalline diamonds, representing equilibration temperatures during the last metasomatic or kimberlitic event, which show overlapping temperatures that are lower compared to thermal gradients of peridotitic xenoliths from the same kimberlites (Fig. 6a). Likewise, the last metasomatic event by saline HDFs, which preceded Group I kimberlite eruptions, had little impact on the temperature and redox conditions of the Kaapvaal lithosphere as a reservoir. However, it likely affected its properties along limited metasomatized veins and their wall rock, as indicated by the chemical and redox zoning between core and metasomatized rim in some individual xenolithic garnets from De Beers Pool kimberlites (Griffin et al., 1999; McCammon et al., 2001; Berry et al., 2013).

5. Summary and conclusions

The De Beers Pool diamonds encapsulate both mineral and high-density fluid (HDF) microinclusions, which help constrain the diamond host rock lithology, the composition of metasomatic agents that impact on this mantle lithology, and the thermal and fO₂ conditions during fluid-rock interaction. Seven of the eight diamonds contain saline HDFs associated with carbonated-peridotite on the basis of their microinclusions of olivine, orthopyroxene, Crpyrope, kosmochlore-bearing diopside, magnesite and phlogopite. Their trace-element patterns show high alkalis (K, Rb and Cs), Ba and LREEs compared to Th, U, Nb and Ta, and are characterized by Ti, Zr, Hf and Y negative anomalies relative to REEs of similar compatibility. Given the low aggregation of the nitrogen of these diamonds (pure Type-IaA IR spectrum), the compositional similarities of their trapped HDFs, and the timing of the Karoo magmatism which elevated the thermal regime of the South African lithosphere, we argue that saline metasomatism and diamond formation took place in proximity to the Group I kimberlite event (\sim 85 Ma), probably just a few million years before their eruption.

Another diamond trapped silicic HDFs. Comparison of the silicic HDFs trace-element pattern with those of saline fluids reveals similar levels of Th, U and Ba, which are all elevated compared to alkalis, a smaller negative Ti anomaly, and positive Zr and Hf anomalies. The nitrogen aggregated nature of this diamond (Type IaAB with 25% of the nitrogen in B-centers) restricts its formation to an earlier and different metasomatic event than that responsible for the formation of saline HDF-bearing diamonds. The state of the nitrogen aggregation in this diamond and the silicic nature of the HDF microinclusions suggest a relation to silica-rich melts that

invaded the southwestern Kaapvaal SCLM prior to, or during, the Karoo magmatism at ca. 180 Ma.

Thermometry and oxythermobarometry for saline metasomatism, based on Mg-Fe exchange between Grt-Opx/Cpx/Ol, the Opx-Cpx thermometer and the saline HDF compositions, yield temperatures between 875–1080 °C and $\Delta \log f O_{2(FMO)}$ of -2.1 to -1.7 at 5 GPa (Fig. 6). They overlap with temperatures recorded by touching inclusion pairs in diamonds from the De Beers Pool kimberlites, which represent the mantle ambient conditions just before eruption, and fO2 conditions of carbonate-bearing melts approaching the EMOG/D buffer. These conditions are lower by 150-250 °C and higher by about 1 $\log fO_2$ unit compared to $P-T-fO_2$ gradients recorded by peridotite xenoliths from the same locality. We suggest that incompatible element enriched saline HDFs mediated the metasomatism that preceded Group I kimberlite eruptions in the southwestern Kaapvaal craton, and that their 'cold and oxidized' nature reflects their derivation from a deep subducting slab. This metasomatic event had little impact on the thermal and redox state of the Kaapvaal lithosphere as a reservoir. However, it likely affected its properties along limited metasomatized veins and adjacent wall rocks, in which diamonds could form by isochemical precipitation or redox processes due to disequilibrium between saline HDFs and the local SCLM. To reconcile the temperature and oxygen fugacity discrepancy between inclusions in diamond and xenoliths, we suggest that the xenoliths did not equilibrate during the last saline metasomatic event or kimberlite eruption. Thus the $P-T-fO_2$ gradients recorded by the xenoliths represent pre-existing lithospheric conditions, expressing re-equilibration after the last major thermal event in the Kaapvaal craton - the Karoo magmatism at ca. 180 Ma.

Acknowledgements

We thank W.L. Griffin and S.Y. O'Reilly for the use of the LA-ICP-MS at Macquarie University, P.B. Kelemen, T. Stachel and G.P. Brey for discussions, D. Walker for discussions and an informal review, and the Diamond Trading Company (a member of the DeBeers Group of Companies) for the donation of diamonds used in this study. V. Stagno and D. Frost are thanked for their help with the calculation of the oxygen fugacity of the HDFs. YW and SG thank the US NSF for support (grants EAR13-48045 and EAR17-25323), and ON thanks the German-Israeli Foundation for Scientific Research and Development (grant GIF I-1239-301.8/2014). This is Lamont-Doherty Earth Observatory contribution number (# 8200).

Appendix A. Supplementary material

Supplementary material related to this article can be found online at https://doi.org/10.1016/j.epsl.2018.03.014.

References

Armstrong, R.A., 1987. Geochronological Studies on Archaean and Proterozoic Formations of the Foreland of the Namaqua Front and Possible Correlates on the Kaapvaal Craton. Witwatersrand University, Johannesburg, p. 274.

Ballhaus, C., Berry, R.F., Green, D.H., 1991. High pressure experimental calibration of the olivine–orthopyroxene–spinel oxygen geobarometer: implications for the oxidation state of the upper mantle. Contrib. Mineral. Petrol. 107, 27–40.

Baptiste, V., Tommasi, A., 2014. Petrophysical constraints on the seismic properties of the Kaapvaal craton mantle root. Solid Earth 5, 45–63.

Bedini, R.M., Blichert-Toft, J., Boyet, M., Albarède, F., 2004. Isotopic constraints on the cooling of the continental lithosphere. Earth Planet. Sci. Lett. 223, 99–111.

Bell, D.R., Gregoire, M., Grove, T.L., Chatterjee, N., Carlson, R.W., Buseck, P.R., 2005. Silica and volatile-element metasomatism of Archean mantle: a xenolith-scale example from the Kaapvaal craton. Contrib. Mineral. Petrol. 150, 251–267.

Bell, D.R., Schmitz, M.D., Janney, P.E., 2003. Mesozoic thermal evolution of the southern African mantle lithosphere. Lithos 71, 273–287.

Berry, A.J., Yaxley, G.M., Hanger, B.J., Woodland, A.B., de Jonge, M.D., Howard, D.L., Paterson, D., Kamenetsky, V.S., 2013. Quantitative mapping of the oxidative effects of mantle metasomatism. Geology 41, 683–686.

- Boyd, F.R., Gurney, J.J., 1986. Diamonds and the African lithosphere. Science 232, 472–477
- Brey, G.P., Köhler, T., 1990. Geothermobarometry in four-phase Lherzolites II. New thermobarometers, and practical assessment of existing thermobarometers. J. Petrol. 31, 1353–1378.
- Carlson, R.W., Pearson, D.G., James, D.E., 2005. Physical, chemical, and chronological characteristics of continental mantle. Rev. Geophys. 43, 24.
- Chevrot, S., Zhao, L., 2007. Multiscale finite-frequency Rayleigh wave tomography of the Kaapvaal craton. Geophys. J. Int. 169, 201–215.
- Creighton, S., Stachel, T., Matveev, S., Hoefer, H., McCammon, C., Luth, R.W., 2009. Oxidation of the Kaapvaal lithospheric mantle driven by metasomatism. Contrib. Mineral. Petrol. 157, 491–504.
- Day, H.W., 2012. A revised diamond–graphite transition curve. Am. Mineral. 97, 52–62.
- Deen, T.J., Griffin, W.L., Begg, G., O'Reilly, S.Y., Natapov, L.M., Hronsky, J., 2006. Thermal and compositional structure of the subcontinental lithospheric mantle: derivation from shear wave seismic tomography. Geochem. Geophys. Geosyst. 7.
- Eaton, D.W., Darbyshire, F., Evans, R.L., Gruetter, H., Jones, A.G., Yuan, X., 2009. The elusive lithosphere–asthenosphere boundary (LAB) beneath cratons. Lithos 109, 1, 22
- Eggler, D.H., Baker, D.R., 1982. Reduced volatiles in the system C-O-H: implications to mantle melting, fluid formation, and diamond genesis. In: Akimoto, S., Manghnami, M.H. (Eds.), High Pressure Research in Geophysics. Center for Academic Publications, Tokyo, Japan, pp. 237–250.
- Evans, T., 1992. Aggregation of nitrogen in diamond. In: The Properties of Natural and Synthetic Diamond. Academic Press, London, pp. 259–290.
- Field, M., Stiefenhofer, J., Robey, J., Kurszlaukis, S., 2008. Kimberlite-hosted diamond deposits of southern Africa: a review. Ore Geol. Rev. 34, 33–75.
- Fouch, M.J., Rondenay, S., 2006. Seismic anisotropy beneath stable continental interiors. Phys. Earth Planet. Inter. 158, 292–320.
- Frost, D.J., McCammon, C.A., 2008. The redox state of Earth's mantle. Annu. Rev. Earth Planet. Sci. 36, 389–420.
- Giuliani, A., Phillips, D., Maas, R., Woodhead, J.D., Kendrick, M.A., Greig, A., Armstrong, R.A., Chew, D., Kamenetsky, V.S., Fiorentini, M.L., 2014. LIMA U-Pb ages link lithospheric mantle metasomatism to Karoo magmatism beneath the Kimberley region, South Africa. Earth Planet. Sci. Lett. 401, 132–147.
- Gray, D.R., Foster, D.A., Meert, J.G., Goscombe, B.D., Armstrong, R., Trouw, R.A.J., Passchier, C.W., 2008. A Damara orogen perspective on the assembly of southwestern Gondwana. Geol. Soc. (Lond.) Spec. Publ. 294, 257–278.
- Griffin, L.W., Shee, R.S., Ryan, G.C., Win, T.T., Wyatt, A.B., 1999. Harzburgite to Iherzolite and back again: metasomatic processes in ultramafic xenoliths from the Wesselton kimberlite, Kimberley, South Africa. Contrib. Mineral. Petrol. 134, 232–250.
- Griffin, W.L., O'Reilly, S.Y., Natapov, L.M., Ryan, C.G., 2003. The evolution of lithospheric mantle beneath the Kalahari craton and its margins. Lithos 71, 215–241.
- Grütter, H.S., Gurney, J.J., Menzies, A.H., Winter, F., 2004. An updated classification scheme for mantle-derived garnet, for use by diamond explorers. Lithos 77, 841–857.
- Gudmundsson, G., Wood, B.J., 1995. Experimental tests of garnet peridotite oxygen barometry. Contrib. Mineral. Petrol. 119, 56–67.
- Hammouda, T., 2003. High-pressure melting of carbonated eclogite and experimental constraints on carbon recycling and storage in the mantle. Earth Planet. Sci. Lett. 214. 357–368.
- Harley, S.L., 1984. An experimental study of the partitioning of Fe and Mg between garnet and orthopyroxene. Contrib. Mineral. Petrol. 86, 359–373.
- Hasterok, D., Chapman, D.S., 2011. Heat production and geotherms for the continental lithosphere. Earth Planet. Sci. Lett. 307, 59–70.
- Holland, T.J.B., Powell, R., 2011. An improved and extended internally consistent thermodynamic dataset for phases of petrological interest, involving a new equation of state for solids. J. Metamorph. Geol. 29, 333–383.
- Ikehata, K., Arai, S., 2004. Metasomatic formation of kosmochlor-bearing diopside in peridotite xenoliths from North Island, New Zealand. Am. Mineral. 89, 1396–1404.
- Izraeli, E.S., Harris, J.W., Navon, O., 2001. Brine inclusions in diamonds: a new upper mantle fluid. Earth Planet. Sci. Lett. 187, 323–332.
- Izraeli, E.S., Harris, J.W., Navon, O., 2004. Fluid and mineral inclusions in cloudy diamonds from Koffiefontein, South Africa. Geochim. Cosmochim. Acta 68, 2561–2575.
- Jacob, D.E., Dobrzhinetskaya, L., Wirth, R., 2014. New insight into polycrystalline diamond genesis from modern nanoanalytical techniques. Earth-Sci. Rev. 136, 21–35.
- Janney, P.E., Shirey, S.B., Carlson, R.W., Pearson, D.G., Bell, D.R., Le Roex, A.P., Ishikawa, A., Nixon, P.H., Boyd, F.R., 2010. Age, composition and thermal characteristics of South African off-craton mantle lithosphere: evidence for a multistage history. J. Petrol. 51, 1849–1890.
- Jourdan, F., Féraud, G., Bertrand, H., Watkeys, M.K., 2007. From flood basalts to the inception of oceanization: example from the ⁴⁰Ar/³⁹Ar high-resolution picture of the Karoo large igneous province. Geochem. Geophys. Geosyst. 8.
- Kelemen, P.B., Hart, S.R., Bernstein, S., 1998. Silica enrichment in the continental upper mantle via melt/rock reaction. Earth Planet. Sci. Lett. 164, 387–406.

- Kessel, R., Pettke, T., Fumagalli, P., 2015. Melting of metasomatized peridotite at 4–6 GPa and up to 1200 °C: an experimental approach. Contrib. Mineral. Petrol. 169. 37.
- Kessel, R., Ulmer, P., Pettke, T., Schmidt, M.W., Thompson, A.B., 2005. The water-basalt system at 4 to 6 GPa: phase relations and second critical endpoint in a K-free eclogite at 700 to 1400 °C. Earth Planet. Sci. Lett. 237, 873–892.
- Klein-BenDavid, O., Logvinova, A.M., Schrauder, M., Spetius, Z.V., Weiss, Y., Hauri, E.H., Kaminsky, F.V., Sobolev, N.V., Navon, O., 2009. High-Mg carbonatitic microinclusions in some Yakutian diamonds a new type of diamond-forming fluid. Lithos 112 (Supplement 2), 648–659.
- Kobussen, A.F., Griffin, W.L., O'Reilly, S.Y., 2009. Cretaceous thermo-chemical modification of the Kaapvaal cratonic lithosphere, South Africa. Lithos 112 (Supplement 2), 886–895.
- Krogh, R., 2000. The garnet-clinopyroxene Fe²⁺-Mg geothermometer: an updated calibration. J. Metamorph. Geol. 18, 211–219.
- Lazarov, M., Brey, G.P., Weyer, S., 2009a. Time steps of depletion and enrichment in the Kaapvaal craton as recorded by subcalcic garnets from Finsch (SA). Earth Planet. Sci. Lett. 279, 1–10.
- Lazarov, M., Brey, G.P., Weyer, S., 2012. Evolution of the South African mantle a case study of garnet peridotites from the Finsch diamond mine (Kaapvaal craton); Part 2: multiple depletion and re-enrichment processes. Lithos 154, 210–223.
- Lazarov, M., Woodland, A.B., Brey, G.P., 2009b. Thermal state and redox conditions of the Kaapvaal mantle: a study of xenoliths from the Finsch mine, South Africa. Lithos 112 (Supplement 2), 913–923.
- Leahy, K., Taylor, W.R., 1997. The influence of the Glennie domain deep structure on the diamonds in Saskatchewan kimberlites. Russ. Geol. Geophys. 38, 481–491.
- Lock, B.E., 1980. Flat-plate subduction and the Cape Fold Belt of South Africa. Geology 8, 35–39.
- Luth, R.W., Stachel, T., 2014. The buffering capacity of lithospheric mantle: implications for diamond formation. Contrib. Mineral. Petrol. 168.
- Macgregor, I.D., 1974. System MgO-Al₂O₃-SiO₂ solubility of Al₂O₃ in enstatite for spinel and garnet peridotite compositions. Am. Mineral. 59, 110–119.
- McCammon, C.A., Griffin, W.L., Shee, S.R., O'Neill, H.S.C., 2001. Oxidation during metasomatism in ultramafic xenoliths from the Wesselton kimberlite, South Africa: implications for the survival of diamond. Contrib. Mineral. Petrol. 141, 287–296.
- McDonough, W.F., Sun, S.S., 1995. The composition of the Earth. Chem. Geol. 120, 223–253.
- Michaut, C., Jaupart, C., 2007. Secular cooling and thermal structure of continental lithosphere. Earth Planet. Sci. Lett. 257, 83–96.
- Miensopust, M., Jones, A.G., Garcia, X., Muller, M., Hamilton, M.P., Spratt, J.E., Evans, R.L., Evans, S.F., Mountford, A., Fourie, C.J.S., Hutchins, D., Ngwisanyi, T., SAMTEX Team, 2006. Lithospheric studies of major Archean cratons and their Proterozoic bounding belts in southern Africa using MT. In: British Geophysical Association Postgraduate Meeting, Edinburgh, 31 August–1 September.
- Navon, O., 1999. Diamond formation in the Earth's mantle. In: Gurney, J.J., Gurney, J.L., Pascoe, M.D., Richardson, S.H. (Eds.), Proceedings of the 7th International Kimberlite Conference, pp. 584–604.
- Navon, O., Hutcheon, I.D., Rossman, G.R., Wasserburg, G.J., 1988. Lunar Planet. Sci. XIX, 827–828.
- Nickel, K.G., Green, D.H., 1985. Empirical geothermobarometry for garnet peridotites and implications for the nature of the lithosphere, kimberlites and diamonds. Earth Planet. Sci. Lett. 73, 158–170.
- Nimis, P., Grütter, H., 2010. Internally consistent geothermometers for garnet peridotites and pyroxenites. Contrib. Mineral. Petrol. 159, 411–427.
- Nimis, P., Taylor, R.W., 2000. Single clinopyroxene thermobarometry for garnet peridotites. Part I. Calibration and testing of a Cr-in-Cpx barometer and an enstatite-in-Cpx thermometer. Contrib. Mineral. Petrol. 139, 541–554.
- O'Neill, H.S.C., Wood, B.J., 1979. An experimental study of Fe–Mg partitioning between garnet and olivine and its calibration as a geothermometer. Contrib. Mineral. Petrol. 70, 59–70.
- Pearson, D.G., Carlson, R.W., Shirey, S.B., Boyd, F.R., Nixon, P.H., 1995. Stabilisation of Archaean lithospheric mantle: a ReOs isotope study of peridotite xenoliths from the Kaapvaal craton. Earth Planet. Sci. Lett. 134, 341–357.
- Pettersson, Å., Cornell, D.H., Moen, H.F.G., Reddy, S., Evans, D., 2007. Ion-probe dating of 1.2 Ga collision and crustal architecture in the Namaqua-Natal Province of southern Africa. Precambrian Res. 158, 79–92.
- Phillips, D., Harris, J.W., Viljoen, K.S., 2004. Mineral chemistry and thermobarometry of inclusions from De Beers Pool diamonds, Kimberley, South Africa. Lithos 77, 155–179
- Rehfeldt, T., Foley, S.F., Jacob, D.E., Carlson, R.W., Lowry, D., 2008. Contrasting types of metasomatism in dunite, wehrlite and websterite xenoliths from Kimberley, South Africa. Geochim. Cosmochim. Acta 72, 5722–5756.
- Rickard, R.S., Harris, J.W., Gurney, J.J., Cardoso, P., 1989. Mineral inclusions in diamonds from Koffiefontein mine. Proc. Int. Kimberlite Conf. 4, 1054–1062.
- Rudnick, R.L., 1999. The thickness and heat production of Archean lithosphere, constraints from xenolith thermobarometry and surface heat flow. In: Mantle Petrology: Field Observations and High-Pressure Experimentation: a Tribute to Francis R. Boyd. In: Spec. Publ. Geochem. Soc., vol. 6, pp. 3–12.

- Shirey, S.B., Richardson, S.H., Harris, J.W., 2004. Integrated models of diamond formation and craton evolution. Lithos 77, 923–944.
- Simon, N.S.C., Carlson, R.W., Pearson, D.G., Davies, G.R., 2007. The origin and evolution of the Kaapvaal cratonic lithospheric mantle. J. Petrol. 48, 589–625.
- Skuzovatov, S., Zedgenizov, D., Howell, D., Griffin, W.L., 2016. Various growth environments of cloudy diamonds from the Malobotuobia kimberlite field (Siberian craton). Lithos 265, 96–107.
- Smith, E.M., Kopylova, M.G., Nowell, G.M., Pearson, D.G., Ryder, J., 2012. Archean mantle fluids preserved in fibrous diamonds from Wawa, Superior craton. Geology 40, 1071–1074.
- Stachel, T., Luth, R.W., 2015. Diamond formation where, when and how? Lithos 220–223, 200–220.
- Stagno, V., Frost, D.J., 2010. Carbon speciation in the asthenosphere: experimental measurements of the redox conditions at which carbonate-bearing melts coexist with graphite or diamond in peridotite assemblages. Earth Planet. Sci. Lett. 300, 72–84
- Stagno, V., Ojwang, D.O., McCammon, C.A., Frost, D.J., 2013. The oxidation state of the mantle and the extraction of carbon from Earth's interior. Nature 493, 84–88
- Sverjensky, D.A., Huang, F., 2015. Diamond formation due to a pH drop during fluid-rock interactions. Nat. Commun. 6, 8702.
- Tappe, S., Foley, S.F., Stracke, A., Romer, R.L., Kjarsgaard, B.A., Heaman, L.M., Joyce, N., 2007. Craton reactivation on the Labrador Sea margins: Ar-40/Ar-39 age and Sr-Nd-Hf-Pb isotope constraints from alkaline and carbonatite intrusives. Earth Planet. Sci. Lett. 256, 433–454.
- Tappert, R., Stachel, T., Harris, J.W., Muehlenbachs, K., Ludwig, T., Brey, G.P., 2005. Diamonds from Jagersfontein (South Africa): messengers from the sublithospheric mantle. Contrib. Mineral. Petrol. 150, 505–522.
- Taylor, W.R., 1998. An experimental test of some geothermometer and geobarometer formulations for upper mantle peridotites with application to the thermobarometry of fertile lherzolite and garnet websterite. Neues Jahrb. Mineral. Abh. 172, 381–408.

- Taylor, W.R., Canil, D., Judith Milledge, H., 1996. Kinetics of lb to laA nitrogen aggregation in diamond. Geochim. Cosmochim. Acta 60, 4725–4733.
- Taylor, W.R., Jaques, A.L., Ridd, M., 1990. Nitrogen-defect aggregation characteristics of some Australasian diamonds: time-temperature constraints on the source regions of pipe and alluvial diamonds. Am. Mineral. 75, 1290-1310.
- Tomlinson, E.L., Jones, A.P., Harris, J.W., 2006. Co-existing fluid and silicate inclusions in mantle diamond. Earth Planet. Sci. Lett. 250, 581–595.
- van Achterbergh, E., Griffin, W.L., Ryan, C.G., O'Reilly, S.Y., Pearson, N.J., Kivi, K., Doyle, B.J., 2002. Subduction signature for quenched carbonatites from the deep lithosphere. Geology 30, 743–746.
- Weiss, Y., Kessel, R., Griffin, W.L., Kiflawi, I., Klein-BenDavid, O., Bell, D.R., Harris, J.W., Navon, O., 2009. A new model for the evolution of diamond-forming fluids: evidence from microinclusion-bearing diamonds from Kankan, Guinea. Lithos 112, 660–674.
- Weiss, Y., Kiflawi, I., Navon, O., 2010. IR spectroscopy: quantitative determination of the mineralogy and bulk composition of fluid microinclusions in diamonds. Chem. Geol. 275, 26–34.
- Weiss, Y., McNeill, J., Pearson, D.G., Nowell, G.M., Ottley, C.J., 2015. Highly saline fluids from a subducting slab as the source for fluid-rich diamonds. Nature 524, 339–342.
- Woodland, A.B., Koch, M., 2003. Variation in oxygen fugacity with depth in the upper mantle beneath the Kaapvaal craton, Southern Africa. Earth Planet. Sci. Lett. 214, 295–310.
- Woodland, A.B., O'Neill, H.S.C., 1993. Synthesis and stability of $Fe_{23}+Fe_{32}+Si_3O_{12}$ garnet and phase relations with $Fe_3Al_2Si_3O_{12}-Fe_{23}+Fe_{32}+Si_3O_{12}$ solutions. Am. Mineral. 78, 1002–1015.
- Wyllie, P.J., 1987. Metasomatism and fluid generation in mantle xenoliths. In: Mantle Xenoliths, pp. 609–621.
- Wyllie, P.J., Ryabchikov, I.D., 2000. Volatile components, magmas, and critical fluids in upwelling mantle. J. Petrol. 41, 1195–1206.